1972

Stability and convergence studies on a numerical model of the Arctic Ocean.

Willems, Robert Cecil.

Monterey, California. Naval Postgraduate School

STABILITY AND CONVERGENCE STUDIES ON A NUMERICAL MODEL OF THE ARTIC OCEAN

Robert Cecil Willems

NAVAL POSTGRADUATE SCHOOL
Monterey, California

THESIS

Stability and Convergence Studies

On a Numerical Model of the Arctic Ocean

by

Robert Cecil Willems

Thesis Advisor: J.A. Galt

March 1972

Stability and Convergence Studies

On a Numerical Model of the Arctic Ocean

by

Robert Cecil Willems
Lieutenant, United States Navy
B.S., Fort Hays Kansas State College, 1965

Submitted in partial fulfillment of the
requirements for the degree of

MASTER OF SCIENCE IN OCEANOGRAPHY

from the

NAVAL POSTGRADUATE SCHOOL
March 1972

ABSTRACT

Complete solutions to the equations of motion are possible using numerical schemes. The model developed by Galt (1972) was investigated for stability and convergence. A series of runs indicated that the scheme, the three level Adams-Bashforth method for the new value of vorticity and then the successive over-relaxation method for the stream function, was stable for transport not exceeding 100 Sverdrups and a time step of one-half pendulum day. Convergence was determined by comparisons, with known analytic solutions, of phase velocity of Rossby waves, and for the steady state conditions, patterns of the stream function and the vorticity. Improved accuracy of the model was attained by using a finer grid.

TABLE OF CONTENTS

LIST OF ILLUSTRATIONS

LIST OF TABLES

I. INTRODUCTION

The study of the dynamics of oceanic flow has been attempted by using the equations of motion. Since solutions to those complex equations in their complete form was not probable it became necessary to simplify them by making highly restrictive assumptions that allowed for some of the functional relationships to be defined as constants and the non-linear terms to be disregarded. Ekman (1905) developed the now classic boundary layer solution, known as the Ekman spiral, which showed the effects of wind stress acting on a free surface. Stommel (1948) was able to reduce the complex equations to a balance between wind stress, a parameterization of friction, and Coriolis force. His solution dramatized the phenomenon of western intensification.

The derivation of the vorticity equation from the vertically integrated equations of motion removed the necessity of defining the pressure field at the surface and simplified the boundary conditions. Munk (1949) developed a solution to a simplified form of the vorticity equation which contained no non-linear terms, was invariant with time, assumed a zonal wind stress, and assumed a constant eddy coefficient. In both solutions the features Stommel observed in his solution were evidenced and, additionally, Munk (1949) observed the counter current region as well.

Development of analytic solutions to the equations of motion necessarily demanded regular, closed boundaries, and for some forms, a constant depth. In each solution mentioned, an ocean of constant depth was assumed or, as in Ekman's solution, the ocean was considered as

unbounded in depth. To study, analytically, ocean basins of irregular boundaries, with inflow and outflow, and variable depth lead to an impossible task.

Early work in developing these solutions was usually attempted for ocean basins that were rectangular in shape. A need to investigate the effects of a laterally sloping boundary was recognized, as evidenced by the more recent work, by Munk and Carrier (1950) which was done on a triangular shaped basin. Studies of the effects of bottom topography on ocean circulation have been presented by Warren (1963) and, more recently, by Veronis (1966). The solutions Veronis developed were to the time dependent, non-advective equations with no friction or wind stress and for a rectangular basin.

It was clearly indicated that with each solution a different phenomenon of oceanic flow could be described using the vorticity equation or the equations of motion. The optimum stiuation, then, would be to obtain a complete solution to these equations so that instead of being restricted to solutions which describe only one of the phenomenon a complete interaction of advection, Coriolis force, friction, and wind stress could be studied as a function of time.

Since a numerical solution to the equations of motion removed the necessity of simplification and allowed for a complete solution, various models have been developed. Usually the only simplifications involved were to specify the density field and friction as constant. More recently Galt (1972) described development of a numerical model of a constant density form of the vorticity equation.

The non-dimensional equations that were used are represented by equations (1) and (2).

Vorticity:

$$\frac{\partial \xi}{\partial t} + h\,\bar{v} \cdot \nabla_H \left(\frac{\alpha\xi + f}{h}\right) = \delta\, \nabla_H^2\, \xi + \nabla_H \times \left(\frac{\bar{\tau}}{h}\right) \qquad (1)$$

Stream function:

$$\nabla \cdot \left(\frac{1}{h}\, \nabla\, \psi\right) = \xi \qquad (2)$$

Where:

ξ = vorticity

h = depth

f = Coriolis parameter

K = lateral kinematic eddy coefficient

$\bar{\tau}$ = wind stress

∇_H = horizontal gradient operator stream function

In this form the non-dimensionalized constants α and δ were defined:

$$\alpha = \psi_o / FL^2 D$$

$$\delta = K/FL^2$$

Where:

ψ_o = a representative value of the stream function

F = a representative value of the Coriolis parameter

D = mean depth

L = the grid length

The non-dimensional wind stress τ was related to τ', the dimensional form, by equation (3).

$$\tau = \tau' \left(\frac{\rho F \psi_o}{L}\right) \qquad (3)$$

Where:

ρ = density

The non-dimensional stream function was then defined:

$$\psi = \psi' (FL^2D) = \psi' \psi_o$$

Using the non-dimensional forms of the equations the model was constructed. The new value of vorticity was obtained by the three level Adams-Bashforth differencing method.

The stream function was then relaxed to within acceptable limits by the method of successive over-relation. This scheme was applied to a polygonal computational molecule.

This computational grid allowed for the specification of irregular boundaries and for inflow and outflow. Newtonian, lateral friction was parameterized in terms of the horizontal Ekman number, K/FL^2.

For models which have been developed it has been necessary to, first, determine their stability and second, to determine their convergence to the true solution. Since complete, analytic solutions were not available, these models were run for conditions which were representative of simplified equations to which solutions existed. Comparisons were then made to assess the validity of the models.

For some finite difference schemes it is possible to mathematically solve for errors generated and determine rates of convergence as well as showing what bounds there must be on the spatial and temporal steps to ensure stability. In referring to the model Galt developed it was not possible to make general calculations for convergence and stability. As indicated by Baer and Simons (1970) a method to investigate numerical stability in a model can be effected by monitoring a conservative property such as energy and total vorticity. The method used to determine

convergence was by a comparison of the patterns of vorticity and the stream function with known analytical solutions. This method, for example, was used by Blandford (1970).

Establishment of the characteristics of Galt's model in terms of stability and convergence was done in two parts; 1): For stability, a form of kinetic energy, total vorticity, and the maximum value of the stream function were monitored; 2): To check convergence a comparison was made between known analytic solutions and the solutions predicted by the model. These comparisons used patterns of the vorticity and the stream function, and of the phase velocity of Rossby waves. These comparisons were made with two different model configurations.

Once the basic shape and boundary conditions were determined the initial input was either constant or variable depth, distribution of the Coriolis parameter, magnitude and direction of the wind stress, stream function and vorticity patterns, and the local rate of change and vorticity one time step back. The parametric specification of density and frictional coefficients, which were assumed constant, and the physical dimensions of a particular configuration were determined by the magnitudes of the non-dimensionalizing constants, ψ_0/FL^2D and K/FL^2. Additionally, for those runs when these constants were zero the dimensions of the model were determined by the distribution of the Coliolis parameter, magnitude of the wind stress, and bottom topography.

The first configuration was a rectangle shape that could only be approximated by the model due to the use of the polygonal molecules for the computational grid. The boundary conditions were set up so as to represent an enclosed basin with free slip boundaries with no friction in the model. The non-linear terms were not used and the wind

stress set to zero so that this solution could be compared to the free wave solutions of Veronis (1966). One run was with constant depth and a variable Coriolis parameter and the other run was with variable depth and a constant Coriolis parameter.

The second series of runs were done using a parallelogram shape which had closed regular boundaries. The east-west boundaries were inclined sixty degrees from the horizontal, measured in a positive sense. This was run with constant depth and a variable Coriolis parameter. The north-south boundaries were set to free slip conditions and the east-west boundaries were set to no slip conditions with friction in the interior. A zonal wind stress set in as a consine function with maximum values at the north-south boundaries. The model did not accurately convert this to the curl of wind stress and, therefore, all successive runs were made with a direct input of the curl of the wind stress. These particular requirements were so that a comparison with a modified solution of Munk and Carrier's (1950) could be made.

The investigation of the effect of reducing the spatial step size was done for both configurations by increasing the number of points and appropriately scaling the input parameters. Reduction of the grid length to one-half was accomplished so as to better define the velocities and western boundary layer.

II. STABILITY ANALYSIS

Baer and Simons (1970) indicated that for the Adams-Bashforth iteration scheme, when used on a non-linear equation, it was sufficient to determine stability for a linear form of that equation since the onset of instability appears to be the breakdown of the linear solutions. Since determination of computational stability was desired it was sufficient, (Baer and Simons [1970]), to monitor the conservative properties which were, kinetic energy, total vorticity, and the maximum value of the stream function. For the stable case, Figure 1, these properties were bounded over the period of integration. Figure 2, the unstable case, indicates some of these values as growing unbounded after a certain integration time. The model's response for the stable situation was a comparatively short spin-up time, as indicated by the values of the properties monitored. The kinetic energy and maximum value of the stream function reached a maximum value at this time and were then observed to oscillate throughout the remainder of the integration time. This response was similar to the results reported by Blandford (1970) for a model in which was specified a lateral viscosity and no slip boundary conditions. Total vorticity reached as maximum value later in the integration then remained constant throughout the remainder of the integration time. For the unstable situation the kinetic energy after a period of time began to grow in an exponential manner with oscillations of the stream function increasing. The vorticity, for this situation, grew steadily throughout the integration time.

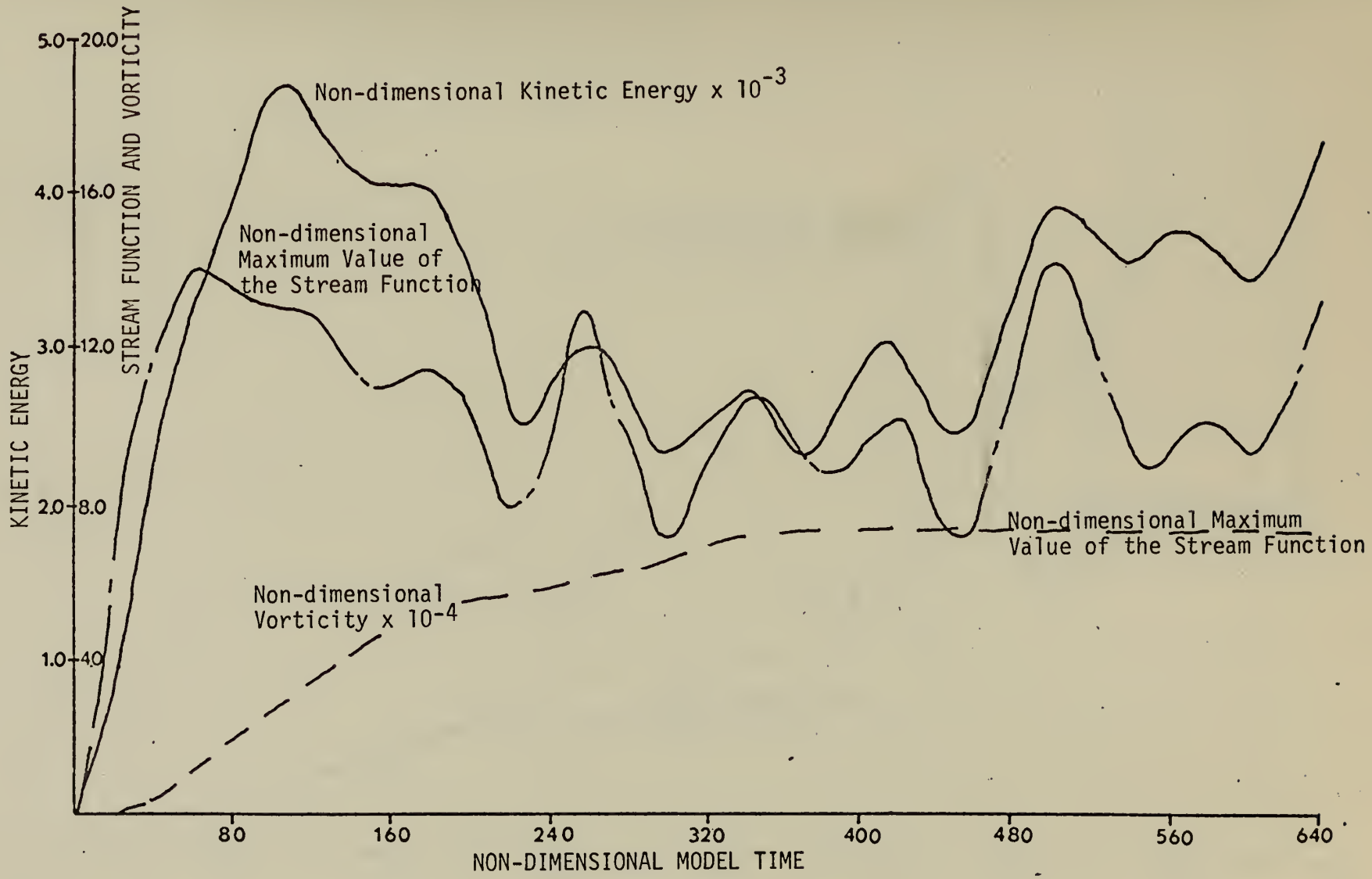

Figure 1. The Stable Case.

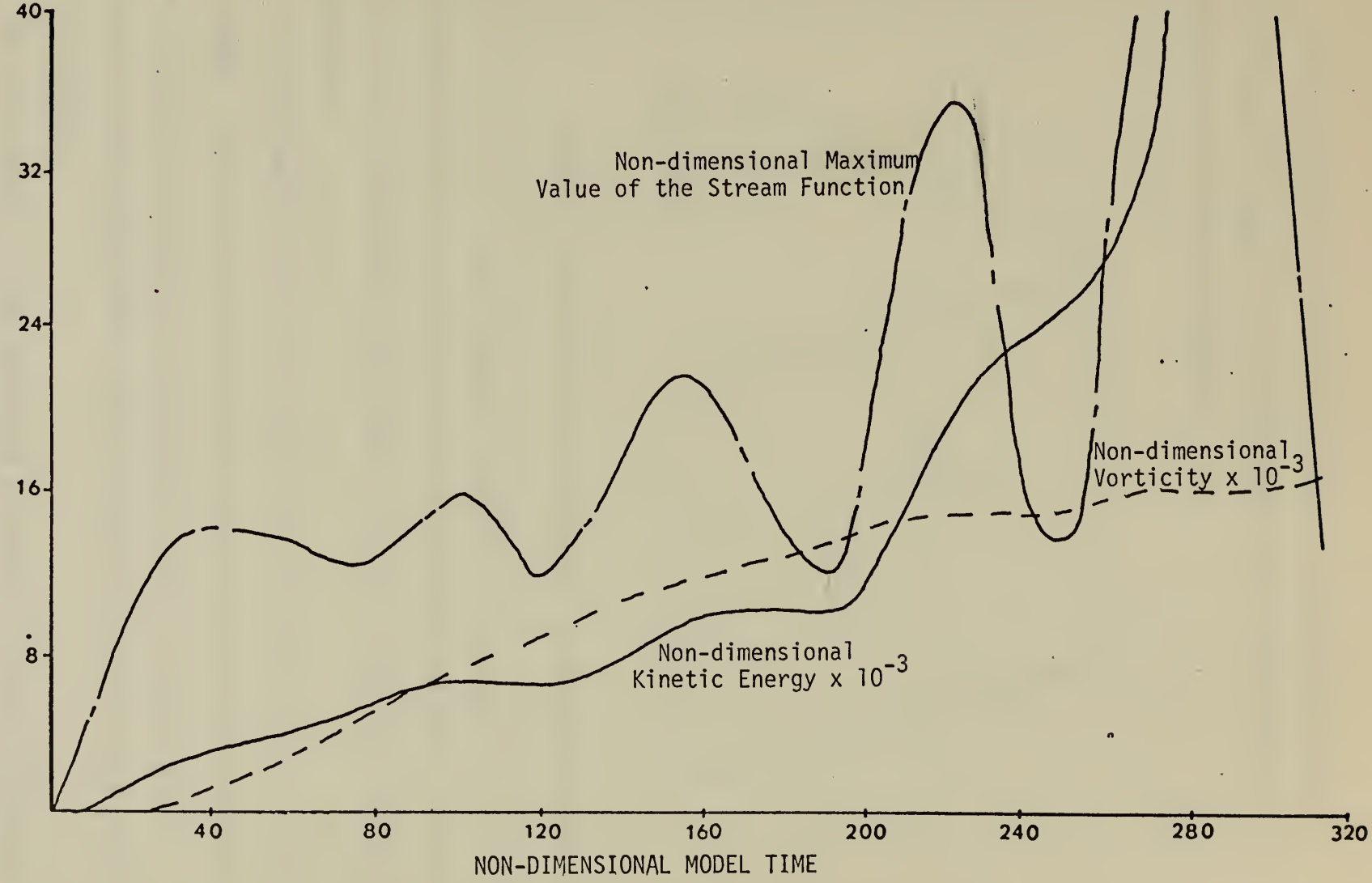

Figure 2. The Unstable Case.

To more accurately determine the limits of stability various conditions were imposed on a constant depth model basin with basic configuration as shown in Figure 3.

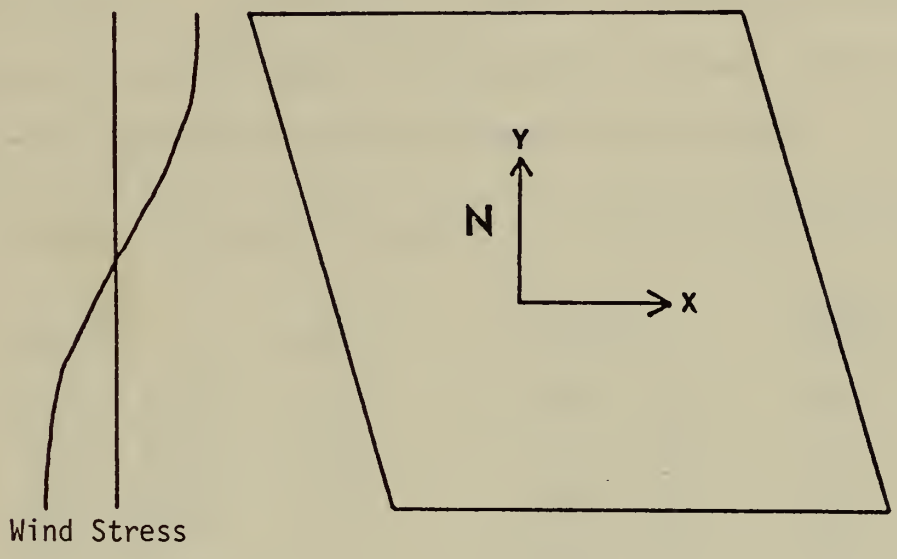

Figure 3. Basic Model Configuration for Stability Analysis

For all but two runs mixed boundary conditions were used with the north and south boundaries being free slip. Of the other two runs, one was run with free slip boundary conditions, the other with no slip boundary conditions.

The distribution of the wind stress over the model basin was zonal in nature. The direction of the wind stress was the cosine function in the north-south direction with the maximum stress in the westward direction at the south boundary and the maximum eastward stress at the north boundary.

The first series of runs were made with the constant (ψ_o/FL^2D) set to zero which resulted in the linear form of the equations. The wind stress was set at a representative value and the Coriolis parameter was

allowed to vary over the constant depth model basin. The physical dimensions of the basin were determined from this distribution. Table I shows the stability for a range of friction, K. For the grid length $L \doteq 4.6 \times 10^5 m$, $F = 10^{-4} sec^{-1}$; K ranges from approximately 7.5×10^8 to $7.5 \times 10^7 cm^2 sec^{-1}$. The effect of varying the magnitude of the wind stress for this test had the effect of varying the transport, and by using large values for the wind stress the model was unstable.

Table I. Stability Dependence on Friction and Time Step.

K/FL^2	DT	KDT/FL^2	STABLE
2.86×10^{-3}	0.5	1.43×10^{-3}	Yes
2.86×10^{-4}	0.5	1.43×10^{-5}	Yes
2.86×10^{-4}	1.0	2.86×10^{-4}	Yes
2.86×10^{-4}	2.0	5.72×10^{-4}	Yes
2.86×10^{-4}	3.0	8.58×10^{-4}	?
2.86×10^{-4}	5.0	1.43×10^{-3}	?
2.86×10^{-4}	7.5	1.71×10^{-3}	No
2.86×10^{-4}	10.0	2.86×10^{-3}	No

Allowing K to remain constant at $7.5 \times 10^8 cm^2 sec^{-1}$ the wind was varied as shown in Table II.

Table II. Stability Dependence on Transport

curl τ_x	DT	STABLE
$-\sin(y)$	0.5	No
0.0	0.5	Yes
$-10^{-4}\sin(y)$	0.5	Yes
$-10^{-2}\sin(y)$	0.5	Yes
$-10^{-1}\sin(y)$	0.5	Yes

By using the non-dimensionalizing coefficient for the wind stress,

$$\tau_x = \tau_x' \left(\frac{\rho F \psi_o}{L}\right)$$

where ρ is density, F a representative value of the Coriolis parameter, L the grid length, ψ_o in Sverdrups ($10^6 m^3/sec$) was determined. The maximum absolute value of the non-dimensional wind stress, τ, was 1.0. with $\rho = 10^{-6}$ grams m^{-3}, $F = 10^{-4} sec^{-1}$, $L = 4.6 \times 10^5 m$ the runs depicted in Table II represent a range of maximum transport from zero to 10^5 Sverdrups.

The effects of non-linearities on the stability of the model are shown in Table III. Keeping K constant at 7.5×10^7, ψ_o/FL^2D was allowed to vary with varying wind stress.

Table III. Stability Dependence on Non-linear Terms and Time Step.

curl τ_x	ψ_o/FL^2D	DT	STABLE
$-10^{-1}\sin(y)$	10^{-2}	1.0	Yes
0.0	10^{-2}	1.0	Yes
$-10^{-1}\sin(y)$	10^{-2}	1.0	No
$-10^{-1}\sin(y)$	10^{-3}	1.0	Yes
$-10^{-1}\sin(y)$	10^{-3}	5.0	?
$-10^{-1}\sin(y)$	10^{-6}	1.0	Yes
$-10^{-1}\sin(y)$	10^{-3}	10.0	No

Inclusion of the non-linear terms by ψ_o/FL^2D where D is the mean model depth, ψ_o ranged from 10^{-2} to 10^2 Sverdrups. This also scaled the magnitude of the wind stress and it ranged from approximately 2×10^{-13} to 2×10^{-9} $m^2 sec^{-2}$ for its maximum values. Similar, unstable, response for large transport was obtained by setting ψ_o/FL^2D to 10.0 which represented approximately 10^5 Sverdrups.

Table IV indicates the final three runs made for determination of computational stability. Again, using the linear form of the equations and K approximately $10^8 cm^2 sec^{-1}$, the maximum transport for the wind stress used was approximately 10 Sverdrups.

Table IV. Stability Dependence on Time Step.

Curl	K/FL^2	DT	STABLE
$-10^{-4}\sin(y)$	5×10^{-4}	1.0	Yes
$-10^{-4}\sin(y)$	5×10^{-4}	5.0	?
$-10^{-4}\sin(y)$	5×10^{-4}	10.0	No

An attempt to compute computational stability was made by using;

$$\left(C \frac{\Delta t}{\Delta x} + K \frac{\Delta t}{(\Delta x)^2}\right) \leq 1.0$$

The term, $C \frac{\Delta t}{\Delta x}$ where C is a characteristic velocity, was not important in the series of linear runs. The term $K \frac{\Delta t}{(\Delta x)^2}$ was computed as shown in Table I with the results of a somewhat larger bounds for Δt. For the transport range of 10 to 100 Sverdrups and a coefficient of friction on the order of $10^8 cm^2 sec^{-1}$ a time step of 10^4 seconds ensured stability. This represented a one-half pendulum day. The effects of the different boundary conditions mentioned previously was to change only the model spin up time. This observation was similar to that reported by Blandford (1970).

III. ROSSBY WAVE PROPAGATION

Convergence of the model to a steady state analytic solution was determined by allowing the model to generate time dependent, free wave solutions and allowing the transients to die out leaving only the steady solution. These Rossby waves can occur in an ocean basin and are of two types. The classical Rossby wave can exist in a constant depth ocean due to the change in the Coriolis parameter with latitude. Considering the situation where there is no friction and no wind stress, with the Coriolis parameter increasing from south to north, a Rossby wave will tend to propagate along lines of a constant Coriolis parameter. For this case, then, the wave would propagate in an east to west direction.

The second type of Rossby wave that can exist in an ocean basin is the topographic Rossby wave. Consider, now, a constant Coriolis parameter but with a simply varying depth which increases from east to west. The topographic Rossby wave will propagate as before except now along lines of constant depth in an east-west direction. For a simply varying depth, increasing from east to west the topographic Rossby waves will propagate from south to north across the ocean basin. These waves can be described by solutions to the potential vorticity equation,

$$\frac{\partial \xi}{\partial t} + \bar{v} \cdot \nabla \left(\frac{f}{h}\right) = ; \quad \xi = \text{vorticity} \qquad (4)$$

Considering that potential vorticity is conserved following a particle of water, equation (4) states that for free wave solutions the second term is zero, that is, f/h is constant. Using equation (4), Veronis (1966) developed a time dependent, harmonic, constant depth solution

for the stream function, ψ (x,y,t).

$$\psi = \psi_0 \sin(\lambda x + \omega t) \sin\alpha x \sin\gamma y \text{ (Veronis[1966])} \qquad (5)$$

Equation (5) describes sinusoidal waves propagating across a basin in the -x direction enclosed in a sine envelope. For the first mode in the x and y directions the following constants were defined:

λ = $\beta/2$

α = π/L

γ = π/M

ω = $\beta/2[\alpha^2 + \gamma^2]^{\frac{1}{2}}$

β = constant = $\frac{\partial f}{\partial y}$

L = basin dimension in x direction

M = basin dimension in y direction

For use in initializing the model non-dimensionalization of equation (5) was necessary. By non-dimensionalizing L, M and λ with a grid length, ΔL, and ω with F, the following non-dimensional constants were defined:

λ' = $[\alpha'^2 + \gamma'^2]^{\frac{1}{2}}$

α' = $(\pi/L)\ \Delta L$

γ' = $(\pi/0.866L)\ \Delta L$

ω' = $\beta\Delta L/2\lambda' F$

ΔL = grid length

L = basin dimension

F = a representative value for the Coriolis parameter.

The phase velocity for this solution is ω/λ which means that the non-dimensional phase velocity is $\omega'/\lambda' = \beta\Delta L/2x^2 F$, or $\beta\Delta L/2F[\alpha'^2 + \gamma'^2]$.

A second solution developed by Veronis (1966) was for a linearized form of equation (4), but with a constant Coriolis parameter and with

variable depth that was assumed to be $h = h_o e^{-kx}$. This solution, equation (6), described sinusoidal wave patterns:

$$\psi = \psi_o \, e^{kx/2} \sin(\lambda y + \omega t) \sin\alpha x \sin\gamma y \qquad (6)$$

propagating in the positive y direction which are enclosed in a sine envelope. The envelope is increasing in an exponential manner in the x direction. Again, for the first mode, the dimensional parameters were defined.

λ = $fk/2\omega$

α = π/L

γ = π/M

ω = $fk/(4[\alpha^2 + \gamma^2] + k^2)^{\frac{1}{2}}$

f = constant Coriolis parameter

L = basin dimension in x direction

M = basin dimension in y direction

Using ΔL to non-dimensionalize L, M, and λ, and ω with F the following parameters were defined:

k' = $k\Delta L$

ω' = $k'/(4[\alpha'^2 + \gamma'^2] + k'^2)^{\frac{1}{2}}$

α' = $(\pi/L)\,\Delta L$

γ' = $(\pi/0.866L)\,\Delta L$

The non-dimensional phase velocity, ω'/λ', was obtained:

$$\omega'/\lambda' = 2k'/(4[\alpha'^2 + \gamma'^2] + k'^2)^{\frac{1}{2}}$$

The rectangle shaped basin which was desired could not be exactly specified as depicted in Figure 4. This model basin shape had sawtoothed east-west boundaries due to the computational grid being made up of

polygonal molecules. Scaling the model basin to physical dimensions was done in the following manner. For the constant depth configuration the model was scaled on the distribution of the Coriolis parameter.

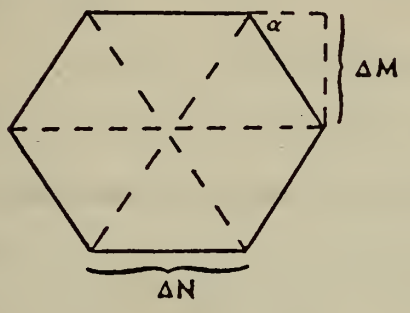

$$\beta = \frac{\partial F}{\partial y} = \frac{\Delta F}{n\Delta M} \quad , \quad n = 9,\ 19$$

$$\Delta F = 0.75 \times 10^{-4}\,\text{sec}^{-1}$$

$$\alpha = 60°$$

using a representative value for $\beta = 1.8 \times 10^{-11}\ \text{-1}\,\text{sec}^{-1}$,

$$\Delta M = \frac{.75}{(9)(1.8\times10^{-11})} = 4.63 \times 10^{5} \text{ meters}$$

$$\Delta N = \frac{\Delta M}{\sin 60°} = 5.35 \times 10^{5} \text{ meters}$$

The configuration for which the Coriolis parameter was constant and the depth varied as in equation (6) determined the physical dimensions of the model in the following manner:

$$h = h_o e^{-kx}$$

$$x = \frac{\ln \frac{h_o}{h}}{k} = n\,\Delta\,N \quad , \quad n = 9,19$$

$$k = 2.2 \times 10^{-7}\,\text{m}^{-1}$$

$$h_o = 3.0 \times 10^{3}\,\text{m}$$

$$h = 1.0 \times 10^{3}\,\text{m}$$

$$\Delta N = 5.56 \times 10^{5}\,\text{m}$$

$$\Delta M = \sin 60°(\Delta N) = 4.83 \times 10^{5}\,\text{m}$$

Since free wave solutions were desired, all of the boundary conditions were set at free slip. The constants K/FL^2 and ψ_o/FL^2D were set to zero so that the model had no friction and so the linear equations could be solved. Since the wind stress was also zero for these runs initialization of the stream function and corticity patterns was

necessary. To accomplish this, the non-dimensionalized solutions developed earlier from equations (5) and (6) were solved at the non-dimensional time 5 and the resulting patterns used as input to initialize the model.

In general, the model propagated the two types of Rossby waves across the basin with the kinetic energy and total vorticity remaining essentially constant. The fluctuations in kinetic energy that were observed had their maximum value when the wave, depicted in Figure 4, reached the center of the basin. This was expected since the waves were propagating in a sine envelope which reached its maximum at the center of the basin. The influence of the boundaries on the waves appeared to cause them to disperse laterally. This observed influence quickly disappeared as the waves moved to the interior of the model

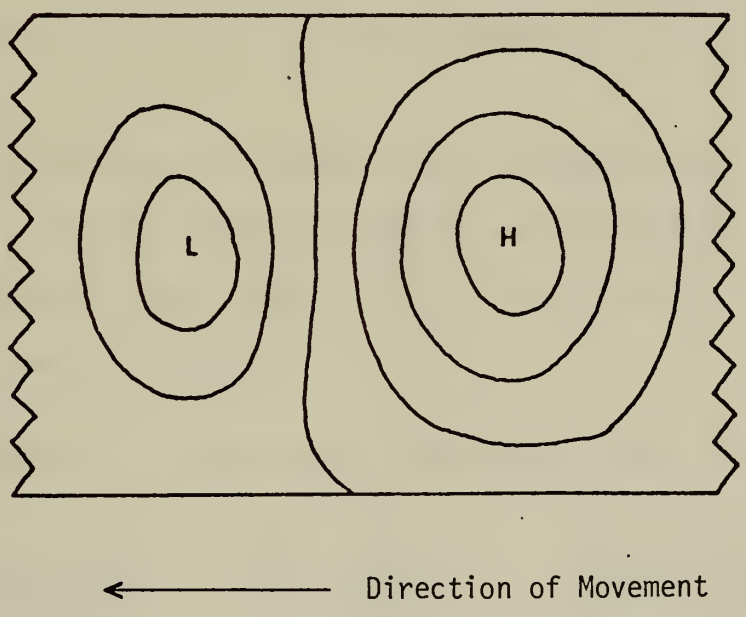

Figure 4. Example of Rossby Wave Propagation.

Reducing the grid length to one-half its former value by doubling the number of points on a side did not change these observed characteristics. Subsequent analysis indicated that these waves were more accurately defined with the decreased grid length.

The phase velocity for both series of runs was determined by using Figures 5 through 8. The first comparisons with analytic solutions are shown in Table V. This was for the configuration denoting a basin of constant depth and with variable Coriolis parameter.

Table V. Comparison of Rossby Wave Velocity.

NUMBER OF GRID POINTS/SIDE	GRID LENGTHS/10 TIME STEPS	NON-DIMENSIONAL PHASE Vel	
		Model	Analytic Solution
10	1.2	.12	.169
20	2.4	.24	.356

The percent error for ten grid points was 29 % and that for twenty grid points was 17 %.

The configuration of a basin with an exponentially varying depth and with a constant Coriolis parameter was analyzed in a similar manner for topographic Rossby waves. Table VI indicates the comparison made with the analytic solution.

Table VI. Comparison of Topographic Rossby Wave Velocity.

NUMBER OF GRID POINTS/SIDE	GRID LENGTHS/10 TIME STEPS	NON-DIMENSIONAL PHASE Vel	
		Model	Analytic Solution
10	1.2	.12	.212
20	3.5	.35	.445

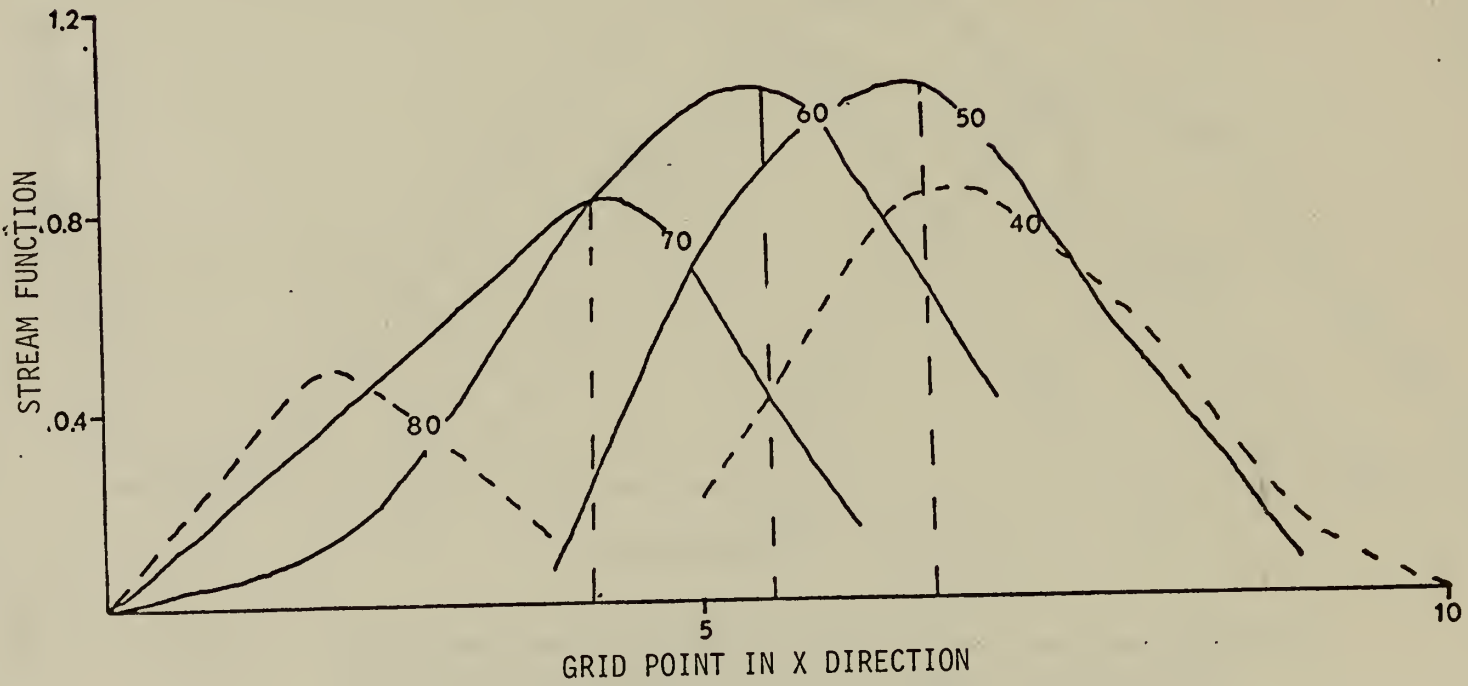

Figure 5. Non-dimensional Stream Function at Every Ten Time Steps for Phase Velocity Determination, the Classic Rossby Wave.

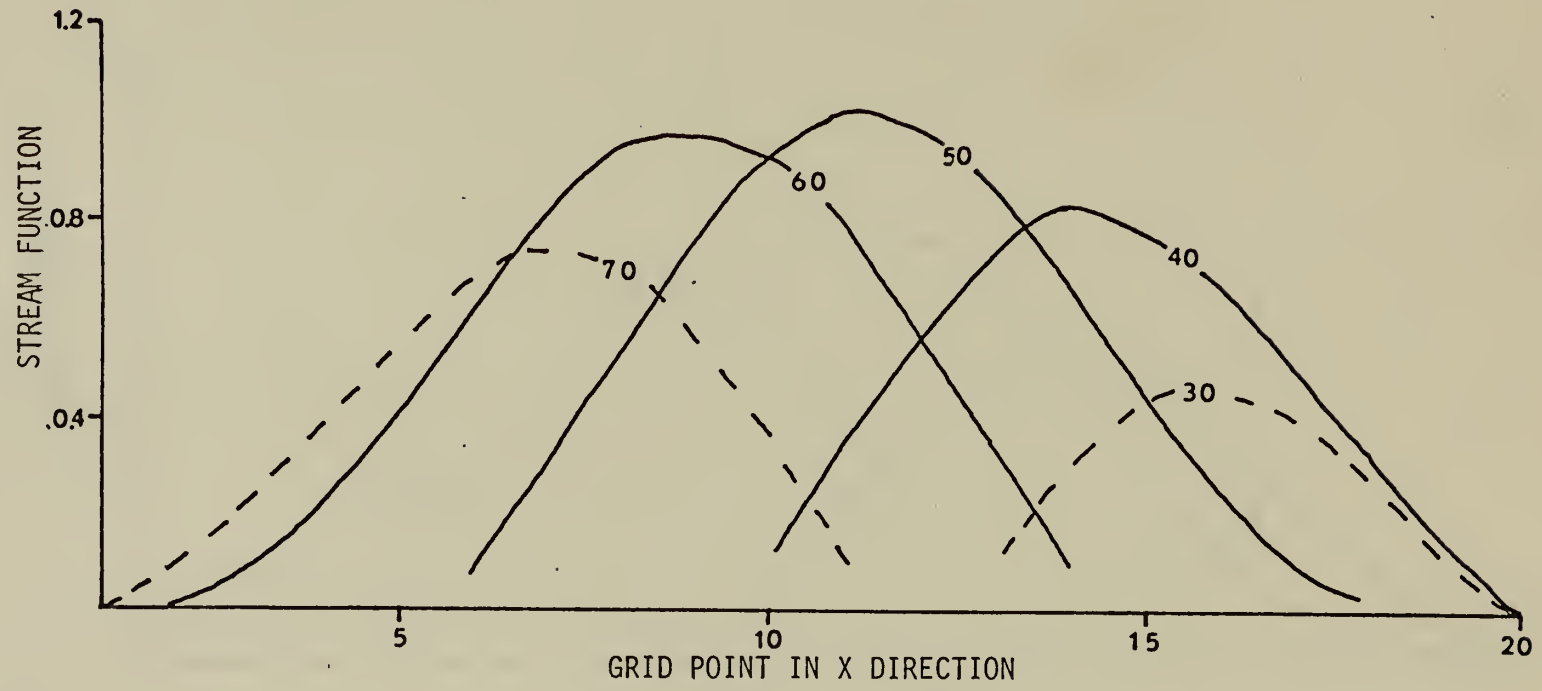

Figure 6. Non-dimensional Stream Function at Every Ten Time Steps for Phase Velocity Determination, the Classic Rossby Wave.

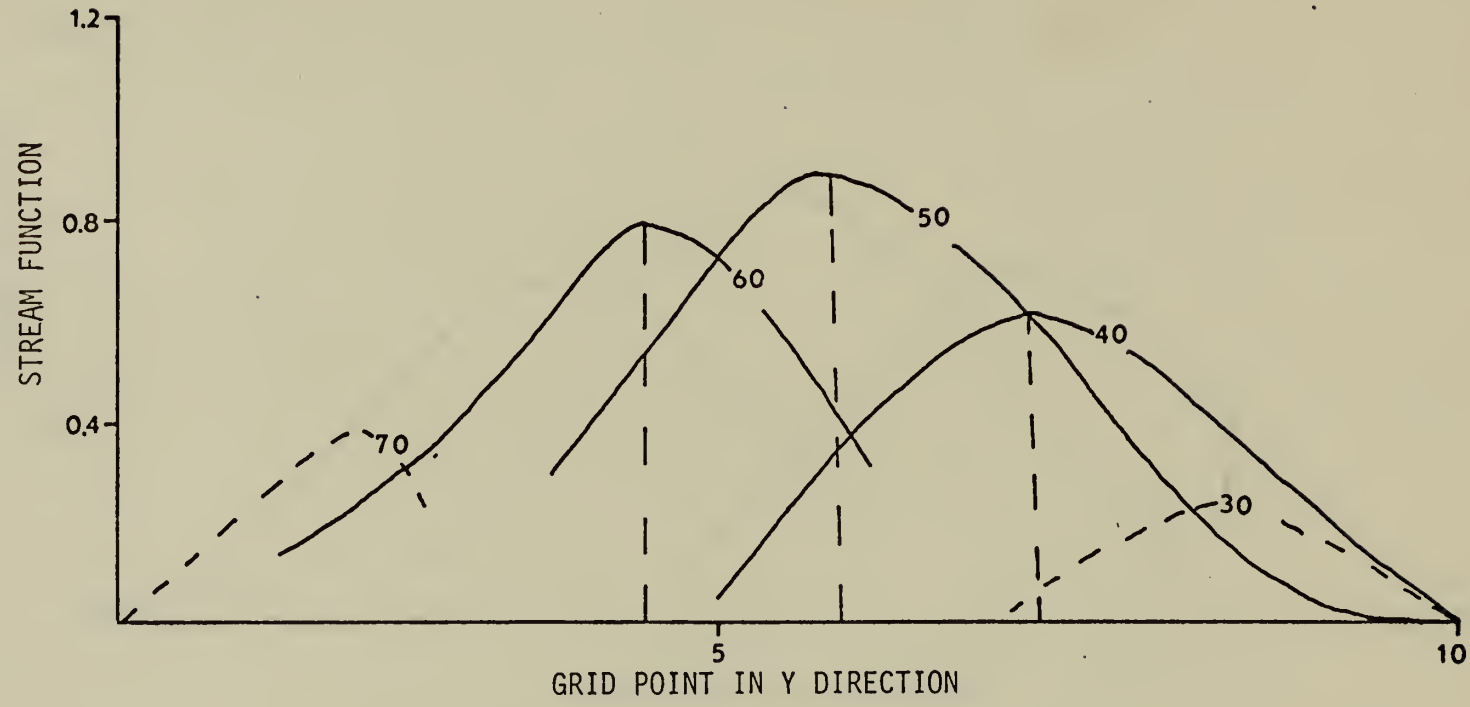

Figure 7. Non-dimensional Stream Function at Every Ten Time Steps for Phase Velocity Determination, the Topographic Rossby Wave.

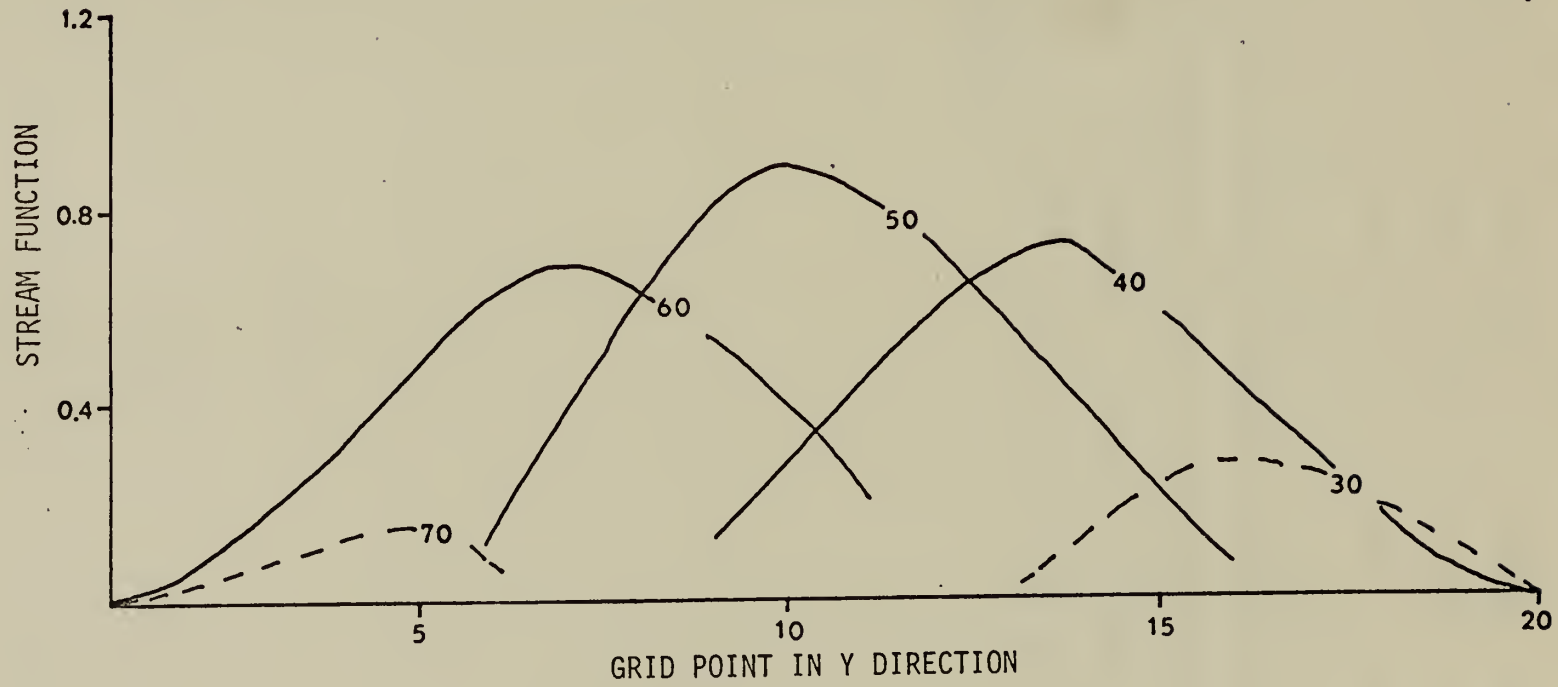

Figure 8. Non-dimensional Stream Function at Every Ten Time Steps for Phase Velocity Determination, the Topographic Rossby Wave.

The same trend was observed in that the percent error for ten grid points was 33 % and that for twenty grid points was 21 %.

This series of runs established a very important trend for the model. Increasing the number of computational points increases the accuracy of the model for the free wave solutions. In approximate terms, doubling the number of computational points very nearly halves the percent error as compared to the known analytic solutions. This determination was subject to graphical interpretation which introduced possible errors. In an attempt to clarify the picture, the figures were normalized with respect to the $\sin\alpha x$ envelope but no significant improvement resulted.

IV. THE STEADY STATE SOLUTION

The assumption that steady state conditions exist in an ocean basin was made by Munk and Carrier (1950) when they derived a beta plane solution on a triangular basin of constant depth. This solution to the vorticity equation balanced frictional effects, Coriolis force, and an assumed wind stress distribution. To make this compatable with the configuration of the numerical model, Figure 9, the dependence of the basin width in the x direction on y was removed so as to make it a constant width. The solution was then corrected for the boundary conditions which were no flow normal to the boundaries. This solution,

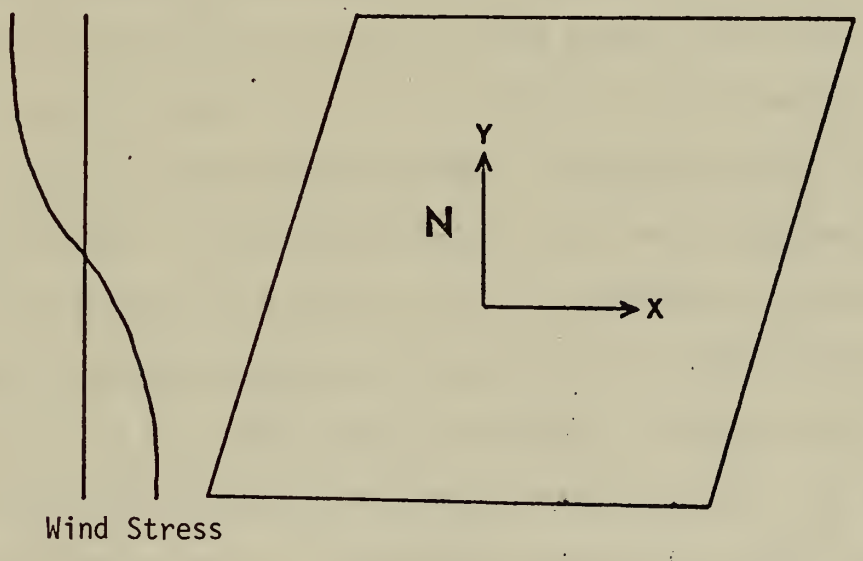

Figure 9. Basic Model Configuration

in non-dimensional form is shown in equation (4);

$$\psi = \sin y[-1.158\{(1-\varepsilon)\cos(\frac{\sqrt{3}}{2}p\alpha + .524) - \varepsilon\sin(\frac{\sqrt{3}}{2}p\alpha)\}e^{(-p\alpha/2)} + 1 - \varepsilon(p\alpha - e^{(p\alpha-1/\varepsilon)} + 1)] \quad (7)$$

with the following parameters defined:

$$\varepsilon = \gamma/\hat{p}$$

$$\hat{p} = (1-\Phi^2 \tan^2\theta)^{-2/3}$$

$$\theta = 60°$$

$$\Phi = 1-1/3(\phi - \phi_o) \tan\phi$$

ϕ_o = latitude at which y = 0

ϕ = latitude at which y = π

$$\alpha = x/\gamma - (y/\gamma) \tan\theta$$

$\gamma\alpha$ = width of the basin

The modified solution is shown in Figures 10 and 11. These patterns were then compared to the steady state reached by the model. To parallel the model with this solution the boundary conditions were set at free slip conditions for the north and south boundaries and no slip for the east and west boundaries. The constant, K/FL^2, curl of the wind stress, and the distribution of the Coriolis parameter were scaled with respect to each other so as to represent a constant depth basin with approximate physical dimensions of 5×10^3km in the x direction and 4.5×10^3km in the y direction, with the curl of the wind stress being distributed as $10^{-4}\sin(y)$ over the basin. The representative value for friction, K, using these values, was $10^8 cm^2/sec$.

As indicated by Figure 12 this configuration reached steady state at about 1×10^7 seconds. This time is when the maximum value of the stream function was essentially at its steady state value with the vorticity and kinetic energy within 95 % of their steady state values. To determine the convergence of this to the analytic solution, patterns of the vorticity and of the stream function were drawn, Figures 13 and 14. The difference between these steady state patterns that the model predicted

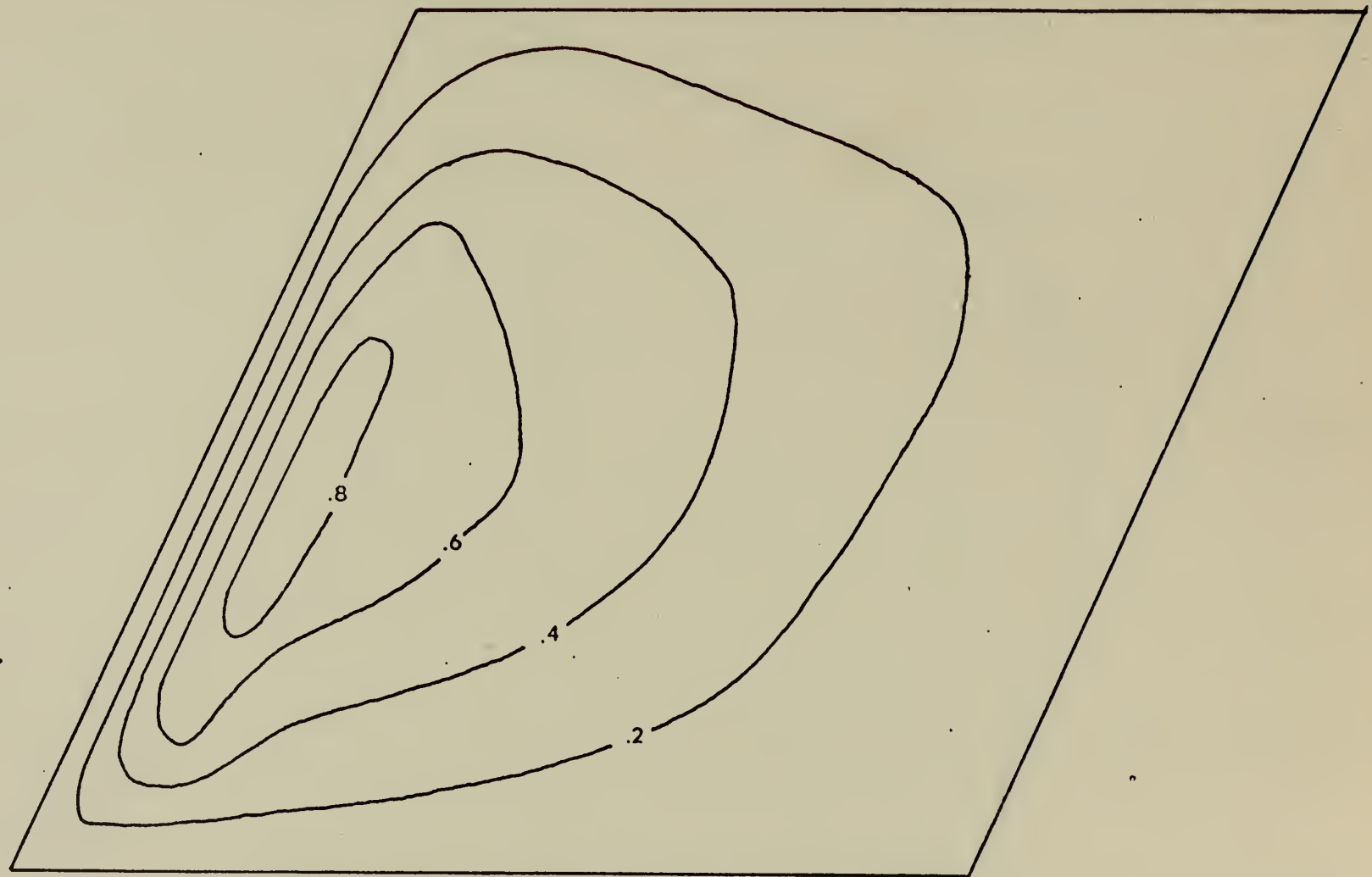

Figure 10. Contoured Values of the Non-dimensional Stream Function for the Modified Solution.

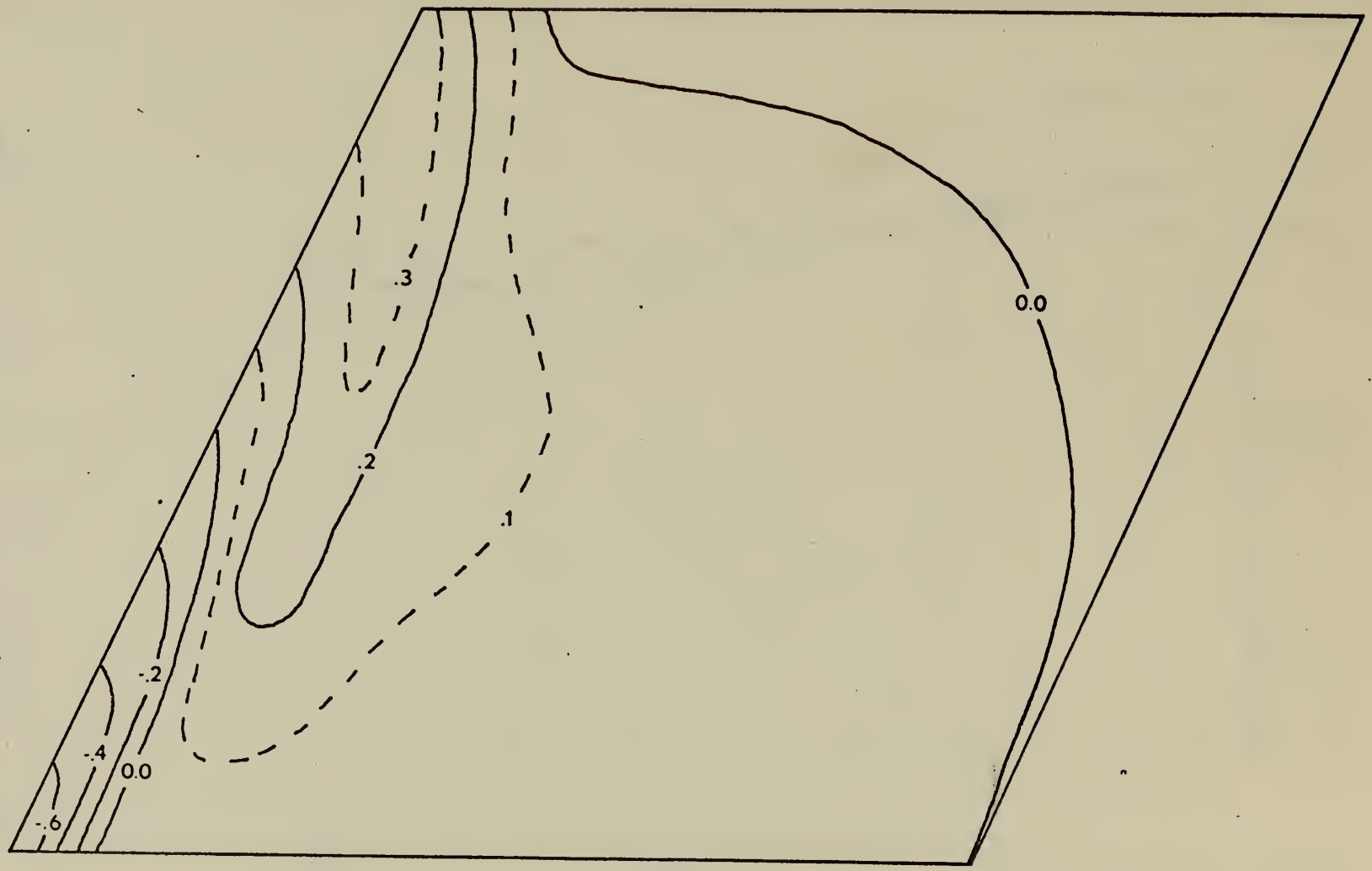

Figure 11. Contoured Values of the Non-dimensional Vorticity for the Modified Solution.

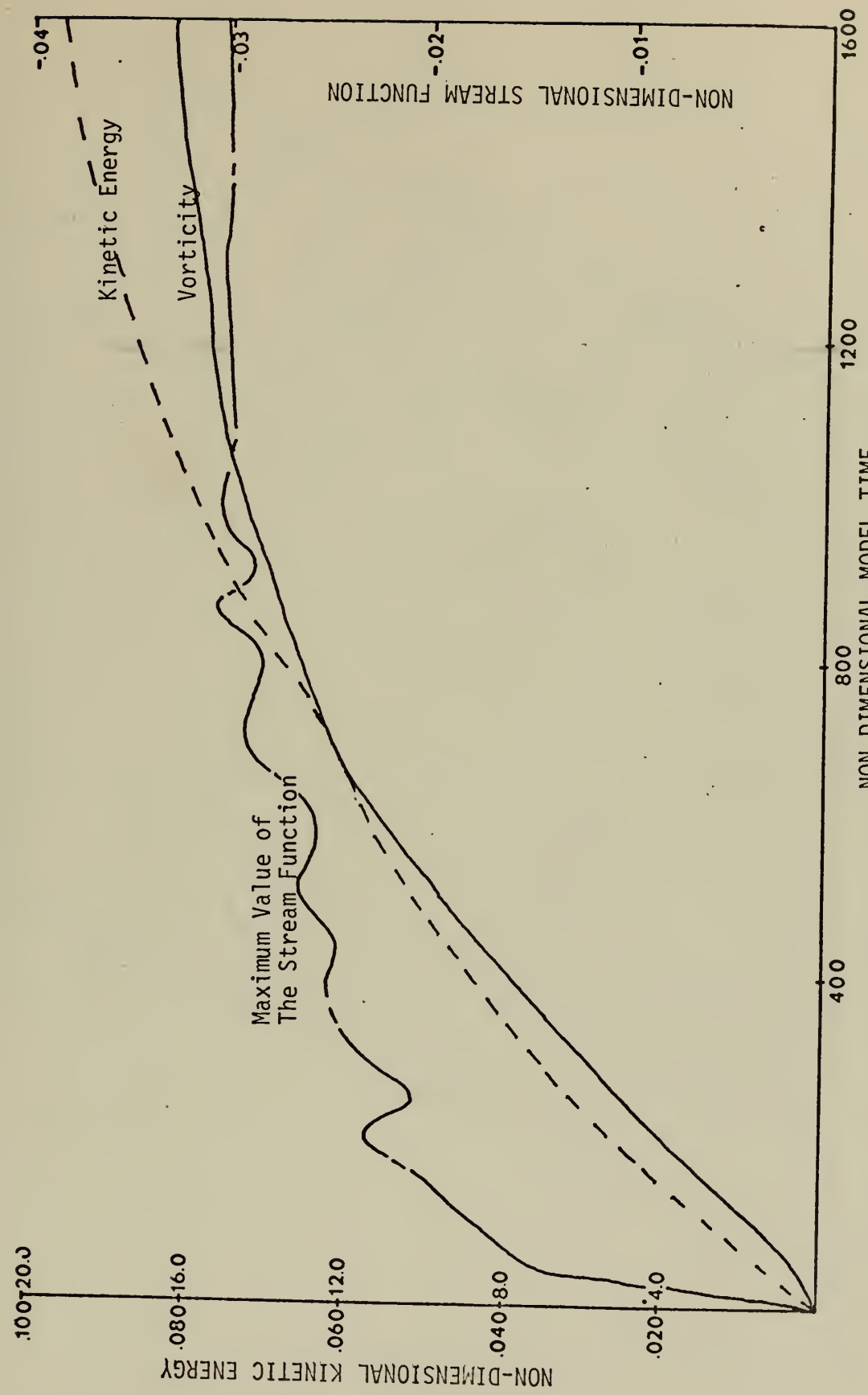

Figure 12. Model Response.

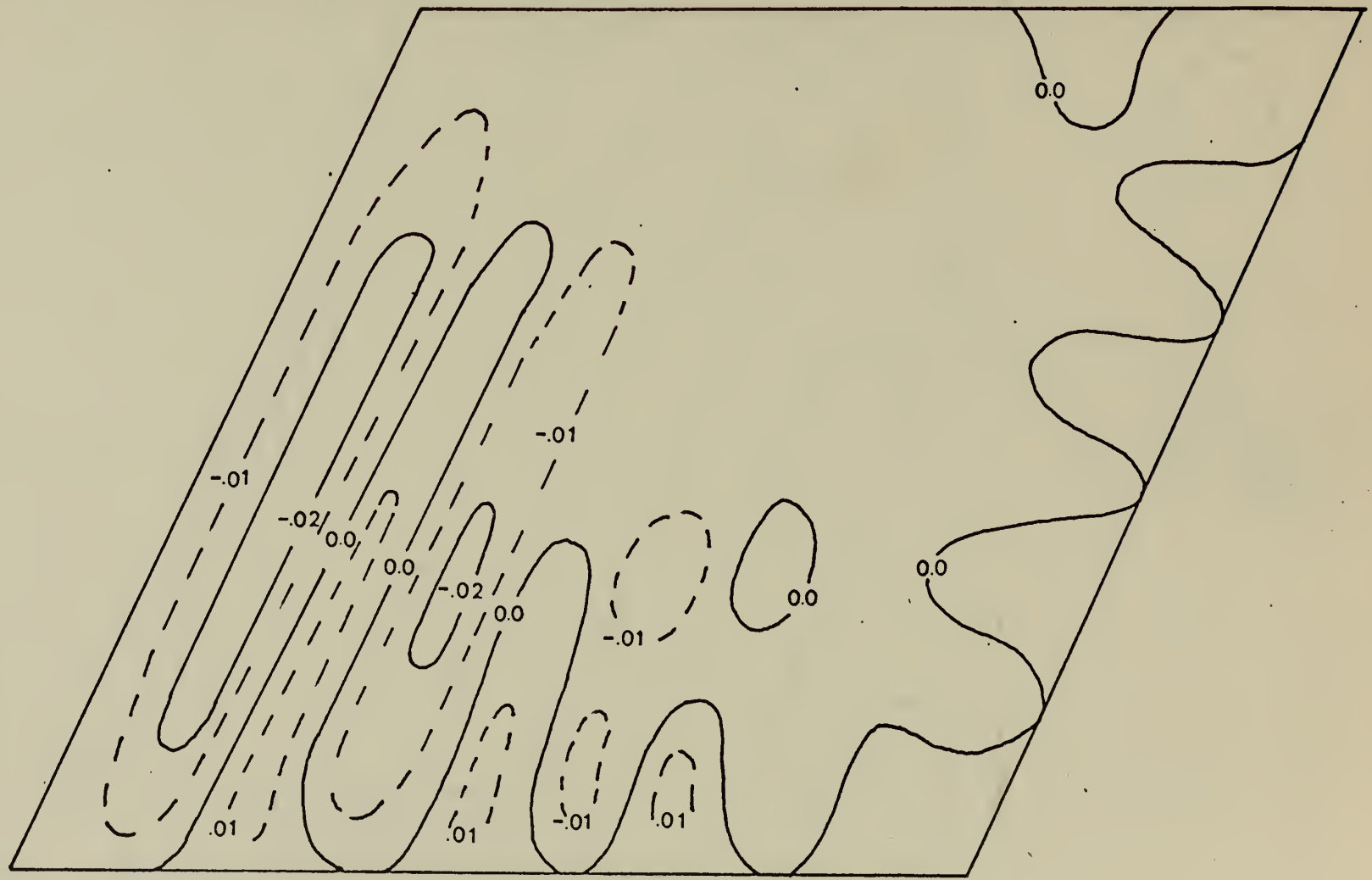

Figure 13. Steady State Pattern of the Non-dimensional Stream Function Predicted by the Model.

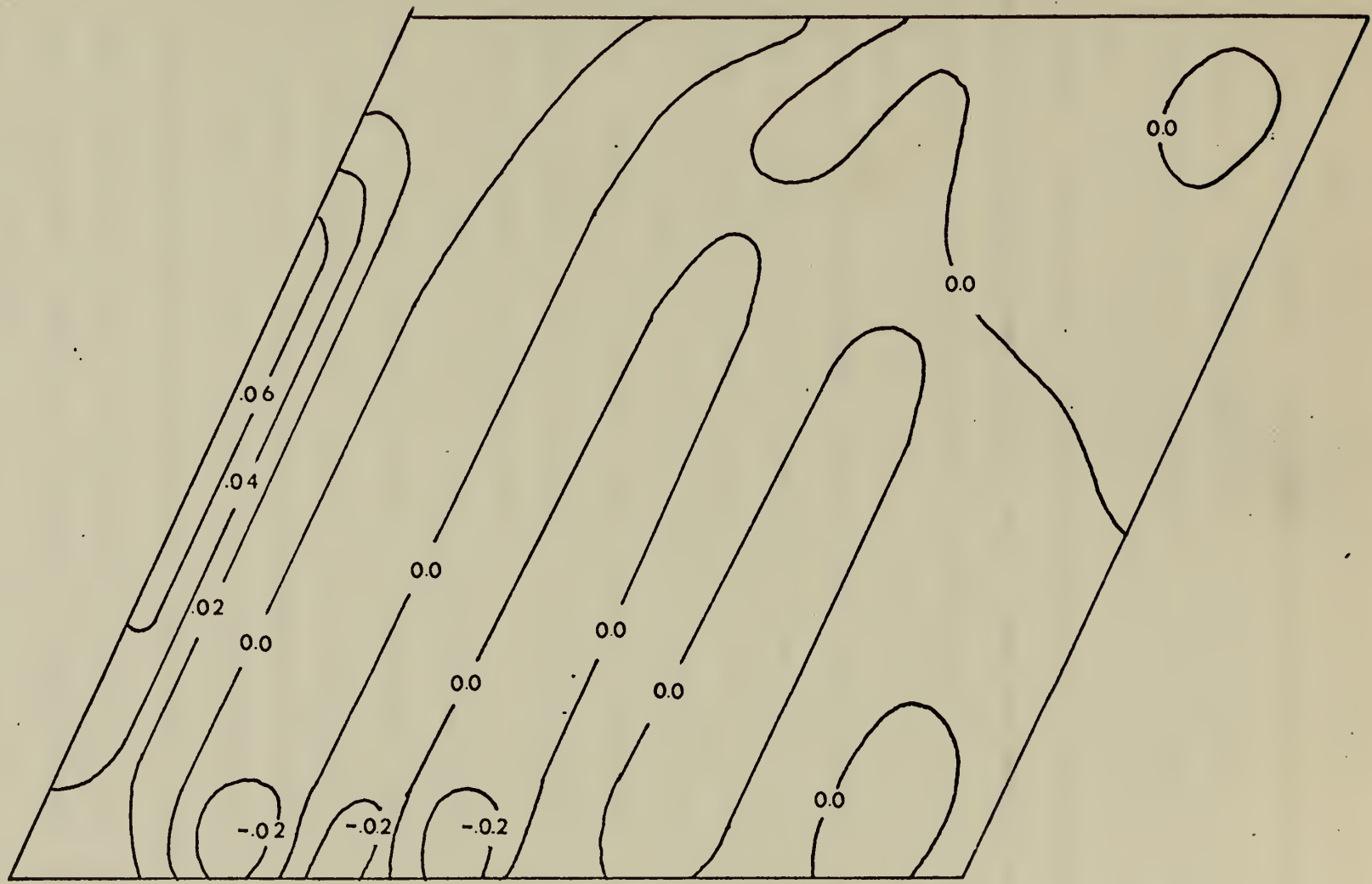

Figure 14. Steady State Pattern of the Non-Dimensional Vorticity Predicted by the Model.

and that of Munk and Carrier could probably be attributed to the difference between the physical conditions which brought the two solutions to a steady state. A numerical model which Gates (1970) used to solve a slightly different form of the equations of motion produced similar steady state patterns. He attributed this to Rossby wave reflections from the boundaries with the most important reflection being the one from the waves which propagated from east to west. These waves diminished in magnitude with each crossing as well as diminishing in magnitude as they propagated through the model. The basic differences, not considering the finite difference methods, between Gates' model and Galt's model were: all boundaries no slip as opposed to mixed free slip/no slip boundaries, and free surface as opposed to a rigid lid. These differences did not cause the two models to vary to any great extent other than a longer spin up time and a phase shift in Galt's model. The most important parallel is that of the type of friction which was lateral and did not include any bottom friction.

Blandford (1970), after considering different combinations of boundary conditions, was able to show by using either free slip or no slip lateral boundaries that bottom friction, expressed as an exponential boundary layer, dissipated more energy than did lateral friction. By including this boundary layer in the solution Blandford noted that the Rossby waves which were generated with model spin up tended to be damped out so that they did not dominate the interior flow. The boundary layer also caused a reduction in the time at which the model reached steady state conditions.

The response of this model, early in the integration, was to develop maximum transport near the center of the basin. This cell soon propagated to the western edge where it dominated the flow as the boundary layer.

After the boundary layer was established, Rossby waves began to initialize in the southeast corner and propagate to near the western boundary. These inertial waves remained near the southern boundary and became established in the flow as the weaker counter current region. Gates reported observations on these waves obtaining the phase velocity of 5.30 meters/sec for their westward component. These waves, depicted in Figures 15 and 16, had as their western component of the phase velocity 5.34 meters/sec for the larger grid and 4.83 meters/sec for the smaller grid.

To better define the phenomenon observed in Galt's model, a reduction of the spatial step size was attempted. Already determined, in Section II, was the improved accuracy of the solution with a smaller grid length. The response of the model for the stream function for different grid lengths, ΔL, was observed in Figure 17 as being a higher maximum value for $(1/2)\Delta L$. This difference was not observed in the comparison of kinetic energy, Figure 18. The difference, in the stream function, between $1\Delta L$ and $(1/2)\Delta L$ was attributed to the influence of transients for the larger grid length. A profile of the stream function for the two grid lengths, Figure 19, indicated that for the larger grid length, $1\Delta L$, the solution oscillates eastward of the counter current region. The smaller grid length, $(1/2)\Delta L$, had a well defined boundary current and the weaker counter current region. The transport decreased rapidly eastward of this region with relatively little oscillation. Comparing this profile with the profile of the modified Munk and Carrier solution, Figure 20, it was observed that the model did in fact compare favorably with the analytic solution in its prediction of the western boundary current and the decrease in transport

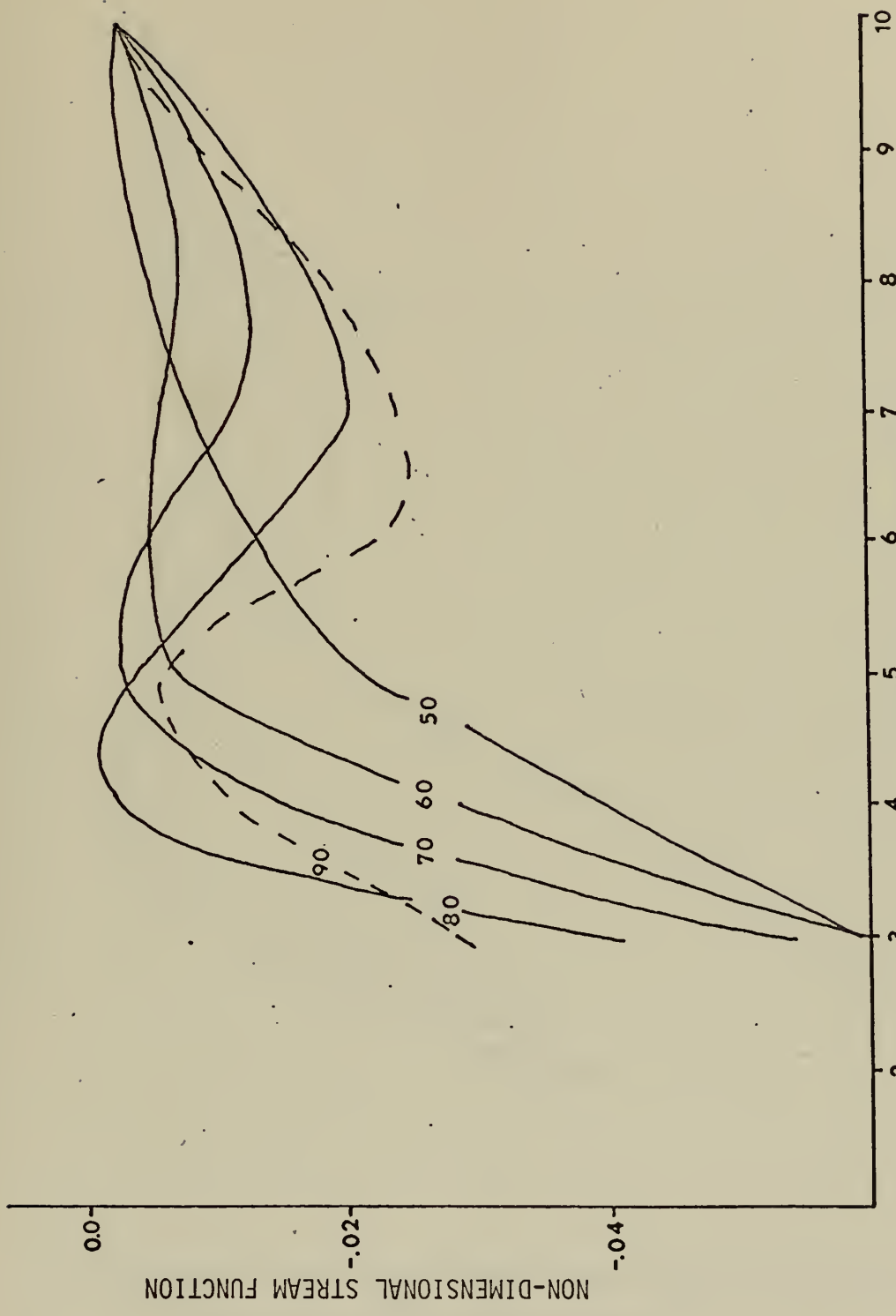

Figure 15. Transient Rossby Wave.

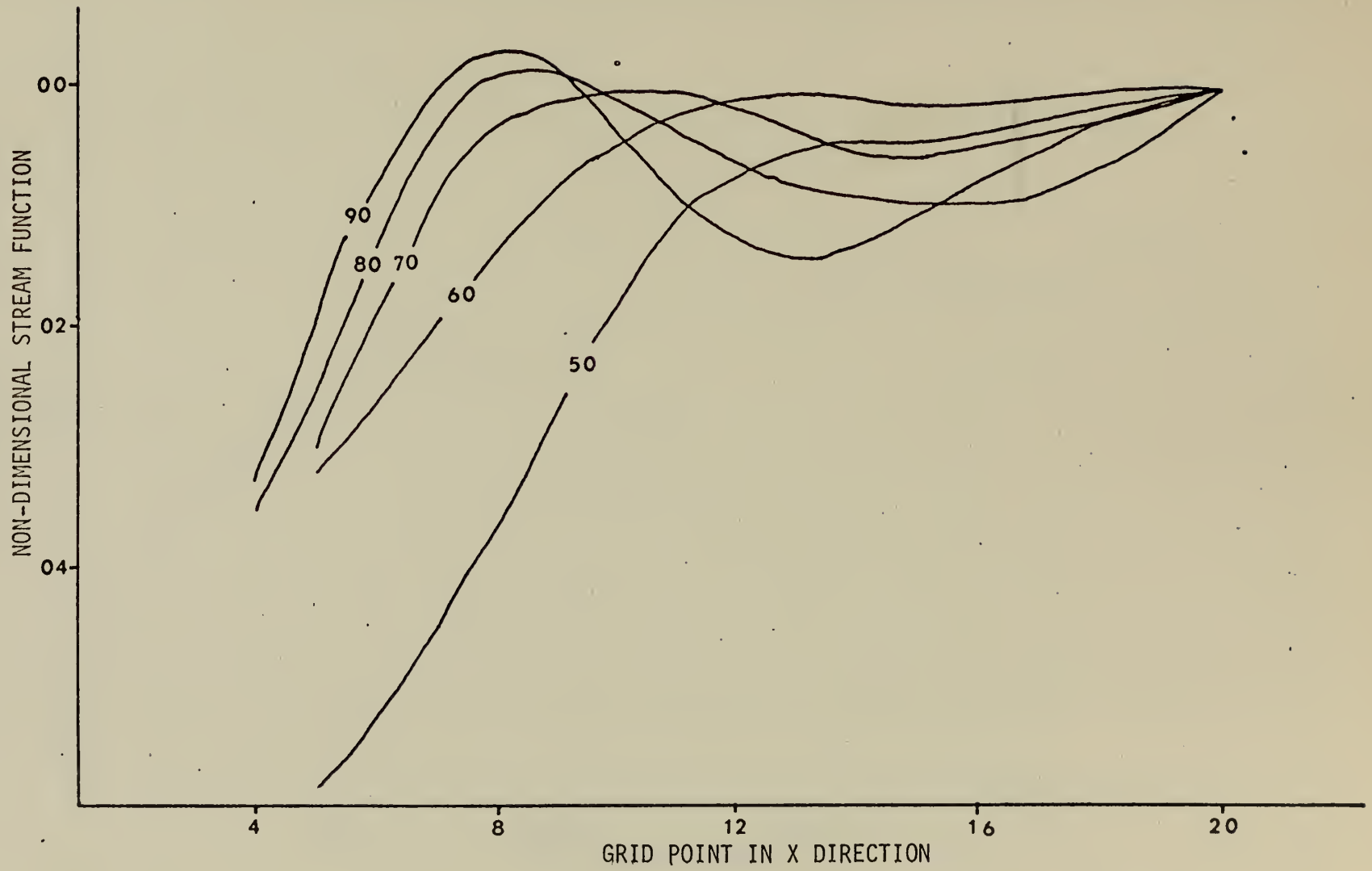

Figure 16. Transient Rossby Wave.

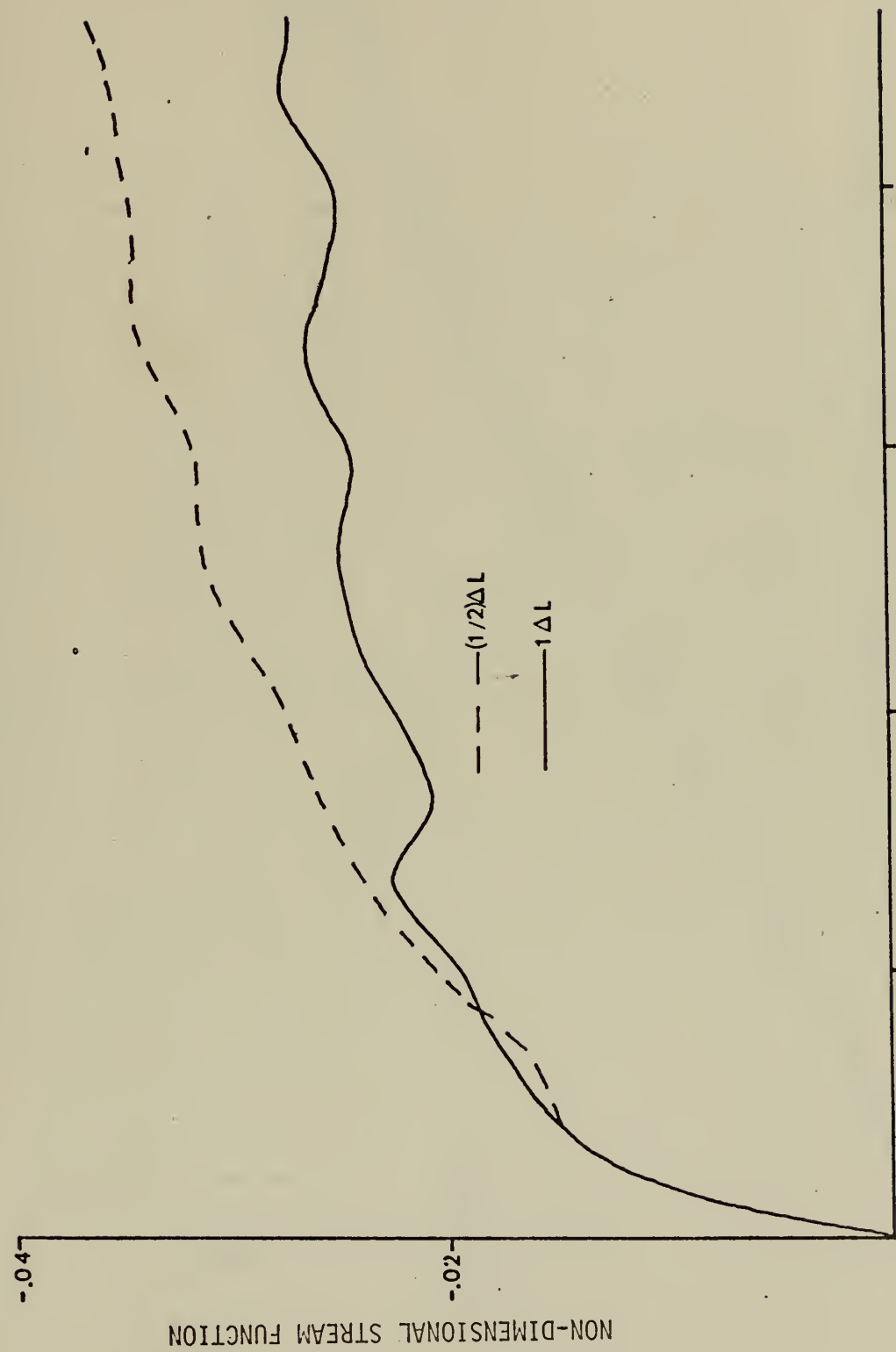

Figure 17. Comparison of the Non-dimensional Stream Function for 1ΔL and 1/2ΔL.

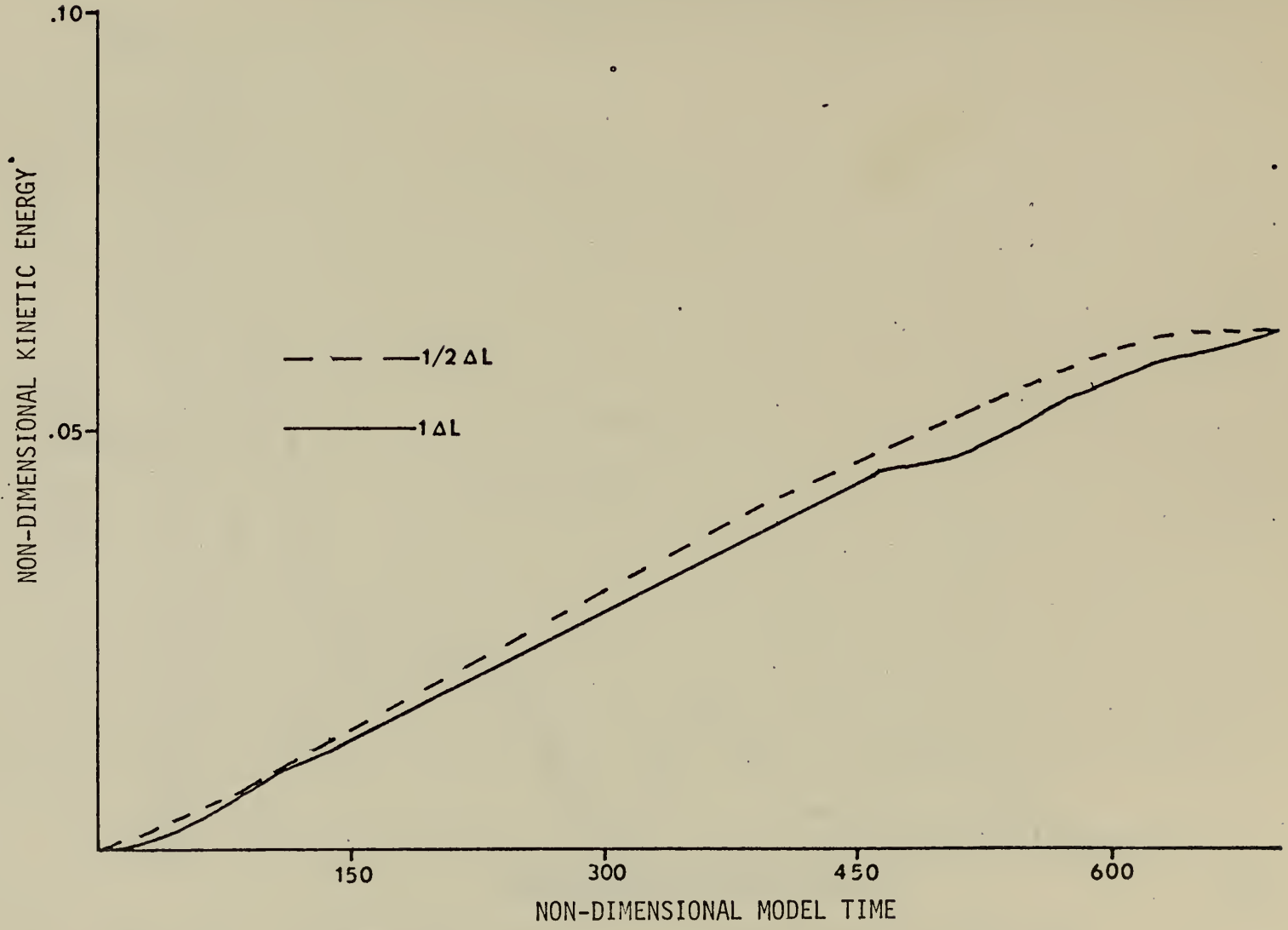

Figure 18. Comparison of the Non-dimensional Kinetic Energy for 1ΔL and 1/2ΔL.

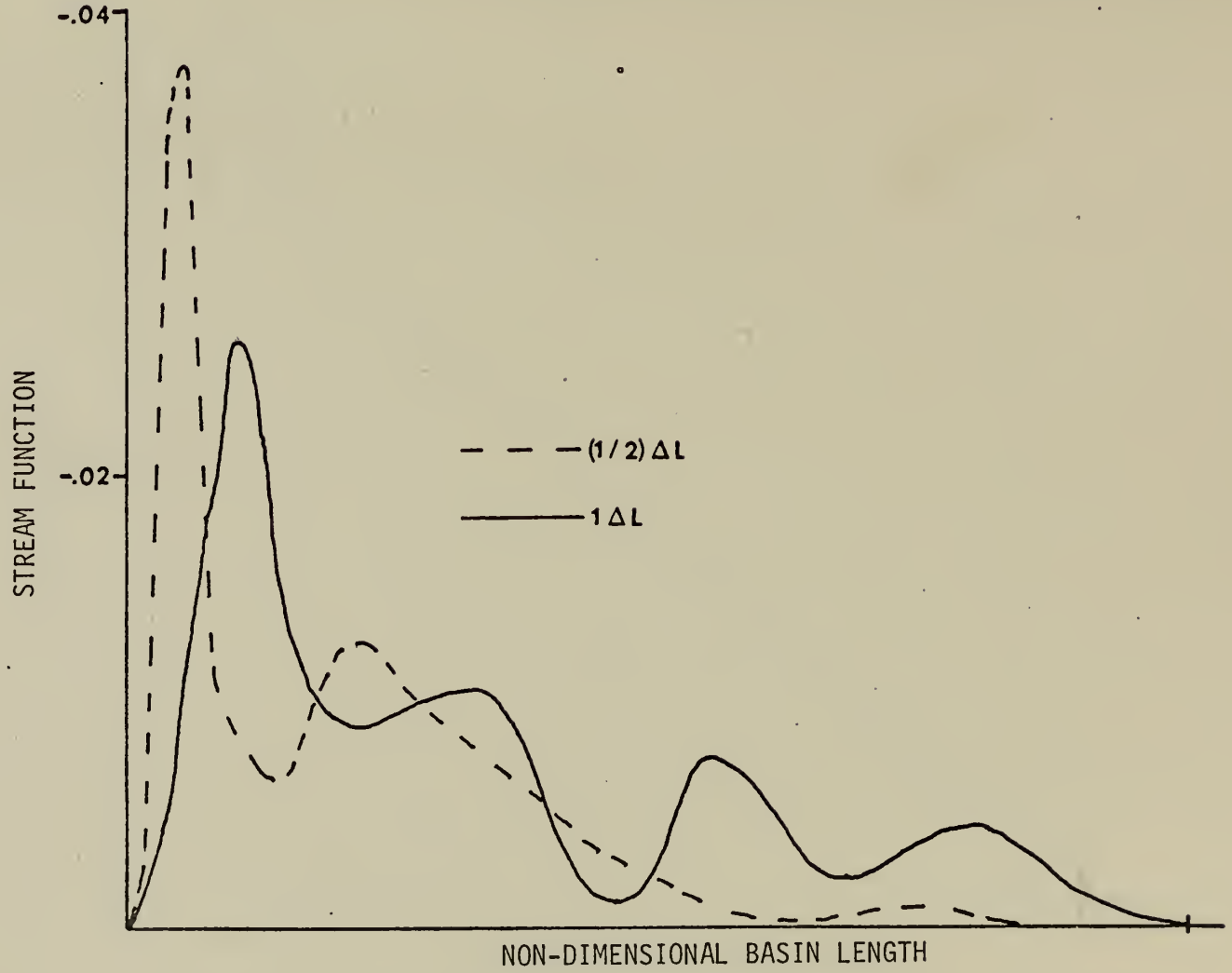

Figure 19. Non-dimensional Profiles of the Stream Function Across the Western Boundary Layer for 1ΔL and 1/2ΔL.

Figure 20. Non-dimensional Profiles of the Stream Function Across the Western Boundary Layer for the Modified Solution.

eastward of the counter current region. The contoured values of the stream function, Figure 21, supported this observation.

The steady state solution generated by the model could be used to acequately indicate oceanic transport. The accuracy of this solution was dependent on grid length, the more accurate solution being obtained using the smaller grid length.

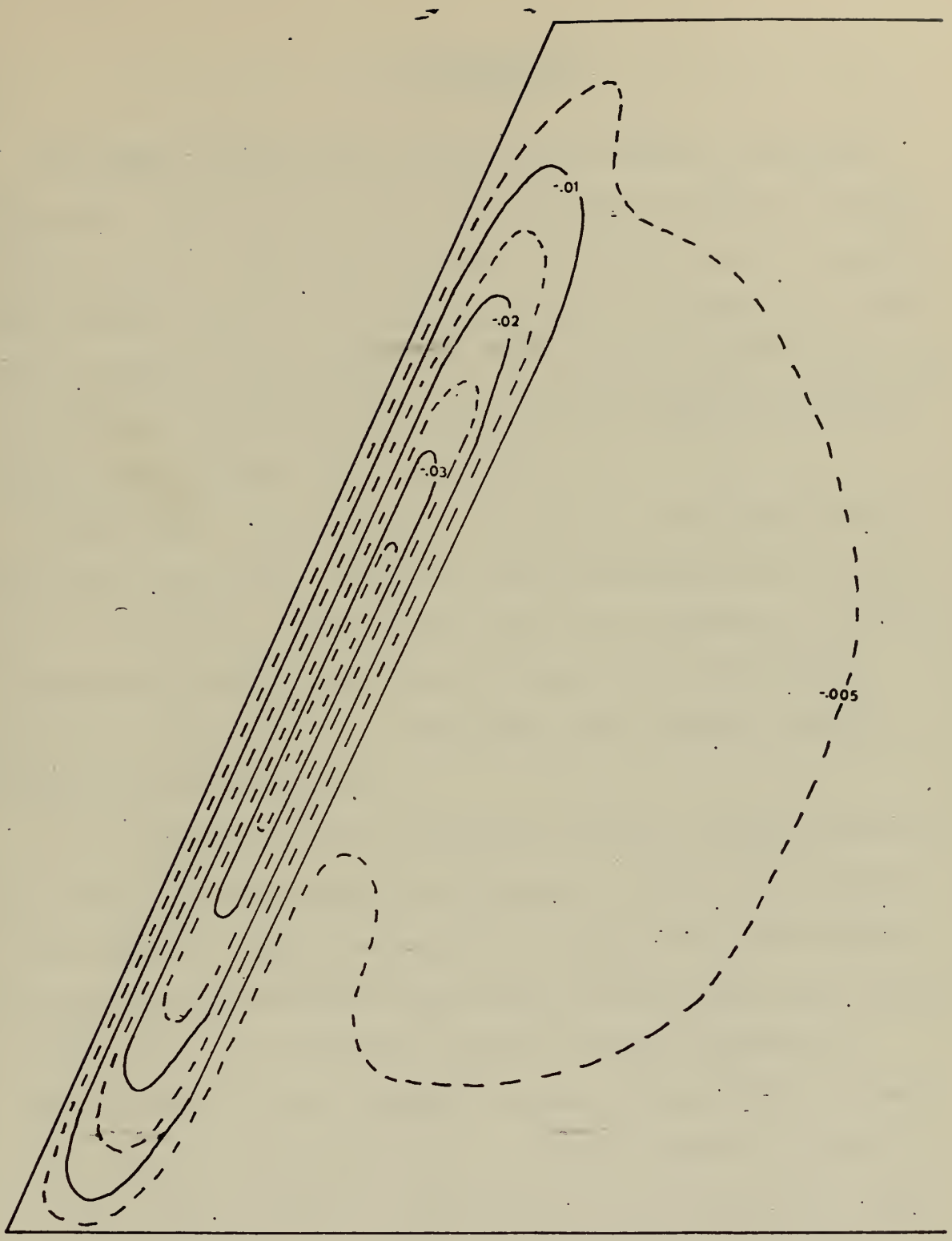

Figure 21. Distribution of the Non-dimensional Stream Function for $1/2\Delta L$.

V. CONCLUSIONS

The model was sufficiently stable for the lengths of integration time used. The model had to be scaled to reflect a transport from zero to 100 Sverdrups with a time step which represented a one-half pendulum day to ensure stability. To reach steady state conditions it was necessary to depend on this factor so that the transients would be damped out.

The curl operation was not accurate enough to produce the correct results when operating on the wind stress.

Rossby waves, either topographic or inertial, were satisfactorily described by the model. The phase velocity was more accurately defined with a refined grid. Although these results were dependent on graphical interpretation this observed trend persisted through the following series of runs in Section III. The errors were significant enough to warrant future investigations.

The steady state solution generated by the model compared favorably with the modified Munk and Carrier solution. To reach this solution a long integration time was necessary. The spin up time was influenced by mixed boundary conditions which caused a longer time to reach steady state conditions. The transient solution the model developed was similar to that which was reported by Gates. This dominating influence could be more accurately described by including some form of bottom friction. These transients became imbedded in the flow and were significant in establishing the counter current region at steady state conditions. The oscillations observed in the stream function profile for larger grid length were due to these transients dominating the steady state flow.

APPENDIX THE FINITE DIFFERENCE EQUATIONS

The specific details of the derivation of the finite difference equations that are given below can be found in Galt (1972). This derivation incompasses a combination of work done by Winslow (1967), Sadourny, Arakawa, and Mintz (1967), and Williamson (1969). By considering a computational molecule, Figure 22, the solution for each term in equation (8) was transformed from a surface integration to a line integration by using Stokes theorem.

$$\frac{\partial \xi}{\partial t} = \underbrace{-h\,\bar{v}\cdot\nabla_H\left(\frac{\alpha\,\xi + f}{h}\right)}_{(1)} + \underbrace{\delta\,\nabla^2\,\xi}_{(2)} + \underbrace{\nabla_H\left(\frac{\bar{\tau}}{h}\right)}_{(3)} \qquad (8)$$

The value of term (1) at point L was considered as an average of the potential vorticity over the molecule times the value of the stream function:

$$\text{potential vorticity } (PV^I) = \left(\frac{\alpha\,\xi^I + F^I}{h^I}\right)$$

$$-h\bar{v}\cdot\nabla_H\left(\frac{\alpha\,\xi + f}{h}\right) = \frac{2}{3\sqrt{3}}\left[\left(\psi^{L-N+L} - \psi^{L+1}\right)\left(\frac{PV^{L-N+1} + PV^{L+1}}{2}\right) + \left(\psi^{L-N} - \psi^{L-N+1}\right)\left(\frac{PV^{L-N} + PV^{L-N+1}}{2}\right) + \left(\psi^{L-1} - \psi^{L-N}\right)\left(\frac{PV^{L-1} + PV^{L-N}}{2}\right) + \left(\psi^{L+N-1} - \psi^{L-L}\right)\left(\frac{PV^{L+N-1} + PV^{L-1}}{2}\right) + \left(\psi^{L+N} - \psi^{L+N-1}\right)\left(\frac{PV^{L+N} + PV^{L+N-1}}{2}\right) + \left(\psi^{L+1} - \psi^{L+N}\right)\left(\frac{PV^{L+1} + PV^{L+N}}{2}\right)\right]$$

The value of term (2) at point L was considered to be the average value over the inner shaded area of Figure 22.

$$\delta\nabla_H^2\xi = \delta\left[\xi^{L+1} + \xi^{L-N+L} + \xi^{L-N} + \xi^{L-1} + \xi^{L-1}\right.$$
$$\left.\xi^{L+N-1} + \xi^{L+N} - 6\xi^{L}\right]$$

Term (3) considered the average values of magnitude and direction of τ along each side of the molecule, then stored as a constant array since it was invariant with time.

$$\nabla_H \times \frac{\overline{\tau}}{h} = \frac{2}{3\sqrt{3}}\left\{\frac{1}{2}\left[\left(\frac{\tau^{L+1}}{h^{L+1}}\right) + \left(\frac{\tau^{L-N+1}}{h^{L-N+1}}\right)\right]\cos\left[\left(\frac{\theta^{L+1} + \theta^{L-N+1}}{2}\right) - \theta^{L+1}\right] + \frac{1}{2}\left[\left(\frac{\tau^{L-N+1}}{h^{L-N+1}}\right) + \left(\frac{\tau^{L-N}}{h^{L-N}}\right)\cos\left[\left(\frac{\theta^{L-N+1} + \theta^{L-N}}{2}\right) + \theta^{L-N+1}\right] + \frac{1}{2}\left[\left(\frac{\tau^{L-N}}{h^{L-N}}\right) + \left(\frac{\tau^{L-1}}{h^{L-1}}\right)\cos\left[\left(\frac{\theta^{L-N} + \theta^{L-1}}{2}\right) - \theta^{L-N}\right]\right.\right.$$
$$\frac{1}{2}\left[\left(\frac{\tau^{L-1}}{h^{L-1}}\right) + \left(\frac{\tau^{L+N-1}}{h^{L+N-1}}\right)\cos\left[\left(\frac{\theta^{L-1} + \theta^{L+N-1}}{2}\right) - {}^{L-1}\right]\right.$$
$$\frac{1}{2}\left[\left(\frac{\tau^{L+N-1}}{h^{L+N-1}}\right) + \left(\frac{\tau^{L+N}}{h^{L+N}}\right)\cos\left[\left(\frac{\theta^{L+N-1} + \theta^{L+N}}{2}\right) - \theta^{L+N-1}\right]\right.$$
$$\left.\left.\frac{1}{2}\left[\left(\frac{\tau^{L+N}}{h^{L+N}}\right) + \left(\frac{\tau^{L+1}}{h^{L+1}}\right)\cos\left[\left(\frac{\theta^{L+N} + \theta^{L+1}}{2}\right) - \theta^{L+N}\right]\right]\right\}$$

The successive over-relaxation procedure was used for equation (2) where the residual was computed by equation (9)

$$\text{Res} = \nabla\left(\frac{1}{h}\nabla\psi\right) - \xi \qquad (9)$$

Res was determined by an average value of $\nabla(\frac{1}{h}\nabla\psi)$ over the inner hexagon, Figure 22.

$$\text{Res} = \frac{4}{3}\left\{\frac{\tau^{L+1}}{h^{L+1}+h^{L}} + \frac{\tau^{L-N+1}}{h^{L-N+1}+h^{L}} + \frac{\tau^{L-N}}{h^{L-N}+h^{L}} + \frac{\tau^{L-1}}{h^{L-1}+h^{L}} + \frac{\tau^{L+N-1}}{h^{L+N-1}+h^{L}}\right.$$

$$\psi^{L}\left[\left(\frac{1}{h^{L+1}+h^{L}}\right) + \left(\frac{1}{h^{L-N+1}+h^{L}}\right) + \left(\frac{1}{h^{L-N}+h^{L}}\right) + \left(\frac{1}{h^{L-1}+h^{L}}\right) + \right.$$

$$\left.\left.\left(\frac{1}{h^{L+N-1}+h^{L}}\right) + \left(\frac{1}{h^{L+N}+h^{L}}\right)\right]\right\} - \xi^{L}$$

The amount of over-relaxation was determined by equation (10).

$$\psi^{L} = \psi^{L} + R(d\psi^{L}) \quad R = 1.48 \tag{10}$$

$$\psi^{L} = \text{Res}\left\{\frac{3}{4}\left[\frac{1}{\left(\frac{1}{h^{L+1}+h^{L}}\right) + \left(\frac{1}{h^{L-N+1}+h^{L}}\right) + \left(\frac{1}{h^{L-N}+h^{L}}\right)}\right.\right.$$

$$\left.\left.\frac{1}{\left(\frac{1}{h^{L-1}+h^{L}}\right) + \left(\frac{1}{h^{L+N}+h^{L}}\right) + \left(\frac{1}{h^{L+N-1}+h^{L}}\right)}\right]\right\}$$

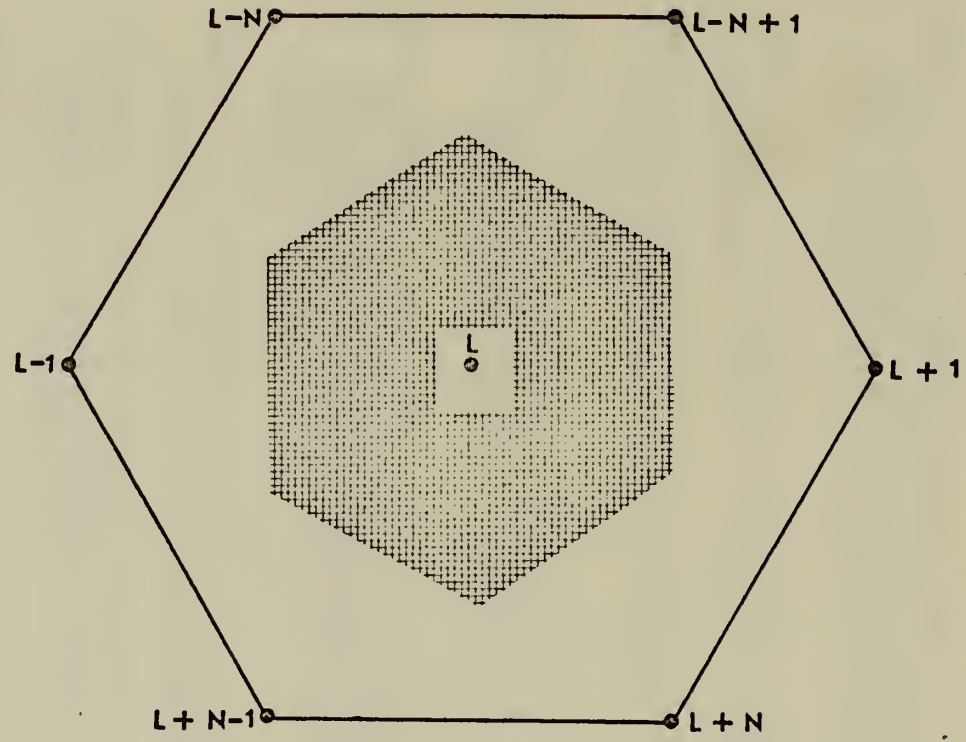

Figure 22. The Computational Molecule.

BIBLIOGRAPHY

1. Blandford, R.R., "Boundary Conditions in Homogeneous Ocean Models," Deep Sea Research, v. 18, pp. 739-751, 25 January 1971.

2. Department of Oceanography Naval Postgraduate School Report (in preparation), The Development of a Homogeneous Numerical Model for the Arctic Ocean, by J.A. Galt, 1972.

3. Gates, W.L., "Effects of Western Coastal Orientation on Rossby-Wave Reflection and the Resulting Large Scale Oceanic Circulation," Journal of Geophysical Research, v. 75(21), 20 July 1970.

4. Munk, W.H., "On the Wind-Driven Ocean Circulation," Journal of Meteorology, v. 7(2), pp. 79-93, 24 September 1949.

5. Munk, W.H., and Carrier, G.F., "The Wind-Driven Circulation in Ocean Basins of Various Shapes," Tellus, v. 2(3), pp. 158-167, 6 March 1950.

6. Rhines, P.B., "Slow Ocsillations in an Ocean of Varying Depth Part 1. Abrupt Topography," Journal of Fluid Mechanics, v. 27(1), pp. 161-189, 4 October 1968.

7. Department of Meteorology University of California, Los Angeles Report 2, Integration of the Non-divergent Barotropic Vorticity Equation with an Icosahedral-hexagonal Grid for the Sphere, by R. Sadourney, A. Arakawa, and Y. Mintz, pp. 1-25, 1 November 1967.

8. Smith, R., "The Ray Paths of Topographic Rossby Waves," Deep Sea Research, v. 18, pp. 477-483, 30 December 1970.

9. Stommel, H., "The Western Intensification of Wind-Driven Ocean Currents," Transaction, American Geophysical Union, v. 29(2), pp. 202-206, 1 September 1948

10. Veronis, G., "Rossby Waves with Bottom Topography," Journal of Marine Research, v. 24(3), pp. 338-349, 25 June 1966.

11. Warren, B.A., "Topographic Influences on the Path of the Gulf Stream," Tellus, v. 15(2), p. 167-184, 1963.

12. Williamson, D., "Numerical Integration of Fluid Flow Over Triangular Grids," Monthly Weather Review, v. 97(12), pp. 885-895 Dec. 1969.

13. Winslow, A.M., "Numerical Solution of the Quasilinear Poisson Equation in a Nonuniform Triangle Mes," Journal of Computational Physics, v. 2, pp. 149-172, 1967.

INITIAL DISTRIBUTION LIST

		No. Copies
1.	Defense Documentation Center Cameron Station Alexandria, Virginia 22314	2
2.	Library, Code 0212 Naval Postgraduate School Monterey, California 93940	2
3.	Department of Oceanography Naval Postgraduate School Monterey, California 93940	3
4.	Asst. Professor J.A. Galt, Code 58Gl Department of Oceanography Naval Postgraduate School Monterey, California 93940	3
5.	Asst. Professor R.T. Williams, Code 51Wu Department of Meterology Naval Postgraduate School Monterey, California 93940	1
6.	LT Robert C. Willems, USN US Naval Destroyer School Newport, Rhode Island	1
7.	Oceanographer of the Navy The Madison Building 732 N. Washington Street Alexandria, Virginia 22314	1
8.	Dr. Ned A. Ostenso, Code 480D Office of Naval Research Arlington, Virginia 22217	1

Security Classification

DOCUMENT CONTROL DATA - R & D

(Security classification of title, body of abstract and indexing annotation must be entered when the overall report is classified)

1. ORIGINATING ACTIVITY (Corporate author)
Naval Postgraduate School
Monterey, California 93940

2a. REPORT SECURITY CLASSIFICATION
Unclassified

2b. GROUP

3 REPORT TITLE
Stability and Convergence Studies on a Numerical Model of the Arctic Ocean

4. DESCRIPTIVE NOTES (Type of report and, inclusive dates)
Master's Thesis; March 1972

5. AUTHOR(S) (First name, middle initial, last name)
Robert Cecil Willems

6. REPORT DATE	7a. TOTAL NO. OF PAGES	7b. NO. OF REFS
March 1972	56	13

8a. CONTRACT OR GRANT NO.	9a. ORIGINATOR'S REPORT NUMBER(S)
b. PROJECT NO.	
c.	9b. OTHER REPORT NO(S) (Any other numbers that may be assigned this report)
d.	

10. DISTRIBUTION STATEMENT
Approved for public release; distribution unlimited.

11. SUPPLEMENTARY NOTES	12. SPONSORING MILITARY ACTIVITY
	Naval Postgraduate School Monterey, California 93940

13. ABSTRACT

Complete solutions to the equations of motion are possible using numerical schemes. The model developed by Galt (1972) was investigated for stability and convergence. A series of runs indicated that the scheme, the three lecel Adams Bashforth method for the new value of vorticity and then the successive over-relaxation method for the stream function, was stable for transport not exceeding 100 Sverdrups and a time step of one-half pendulum day. Convergence was determined by comparisons, with known analytic solutions, of phase velocity of Rossby waves, and for the steady state conditions, patterns of the stream function and the vorticity. Improved accuracy of the model was attained by using a finer grid.

DD FORM 1 NOV 65 1473 (PAGE 1)

S/N 0101-807-6811

Security Classification

A-31408

KEY WORDS	LINK A		LINK B		LINK C	
	ROLE	WT	ROLE	WT	ROLE	WT
Numerical Ocean Model						
Rossby Wave Propagation						
Ocean Circulation						
Ocean Boundary Layers						

Thesis 134782
W5887 Willems
c.1 Stability and convergence studies on a numerical model of the Arctic Ocean.